Boundary Layer Ingestion Fan Stage Internal Flow Analysis and Characterization of Secondary Flow Topography in the Blade Channel

By

Talha Bin Tahir

Reg # 00000317536

Session 2019-2021

Supervised by

Dr. Adeel Javed

A Thesis Submitted to the US Pakistan Centre for Advanced Studies in Energy in partial fulfillment of the requirements of the degree of

MASTERS of SCIENCE in

THERMAL ENERGY ENGINEERING

US-Pakistan Centre for Advanced Studies in Energy (USPCAS-E)

National University of Sciences and Technology (NUST)

H-12, Islamabad 44000, Pakistan

October 2021

THESIS ACCEPTANCE CERTIFICATE

Certified that final copy of MS/MPhil thesis written by **Mr. Talha bin Tahir** (Registration No. 00000317536), of USPCAS-E has been vetted by undersigned, found complete in all respects as per NUST Statues/Regulations, is within the similarity indices limit, and is accepted as partial fulfillment for the award of MS/MPhil degree. It is further certified that necessary amendments as pointed out by GEC members of the scholar have also been incorporated in the said thesis.

Signature: _____

Name of Supervisor Dr. Adeel Javed

Date: _____

Signature: _____

Name of Co-Supervisor Dr. Majid Ali

Date: _____

Signature (HoD TEE): _____

Date: _____

Signature (Dean/Principal): _____

Date: _____

Certificate

This is to certify that work in this thesis has been carried out by **Mr. Talha bin Tahir** and completed under my supervision in US-Pakistan Center for Advanced Studies in Energy (USPCAS-E), National University of Sciences and Technology, H-12, Islamabad, Pakistan.

Supervisor: _____

Dr. Adeel Javed
USPCAS-E
NUST, Islamabad

Co-Supervisor: _____

Dr. Majid Ali
USPCAS-E
NUST, Islamabad

GEC member 1: _____

Dr. Adeel Waqas
USPCAS-E
NUST, Islamabad

GEC member 3: _____

Dr. Adnan Maqsood
USPCASE
NUST, Islamabad

HOD-TEE: _____

Dr. Majid Ali
USPCAS-E
NUST, Islamabad

Principal: _____

Dr. Adeel Waqas
USPCAS-E
NUST, Islamabad

Abstract

The robust performance of transonic fans in the presence of inlet distortions for boundary layer ingesting aircraft poses significant design challenges. This paper presents a numerical optimization strategy for distortion tolerant transonic fan design featuring an improved interaction between the transonic fan tips and the upstream flow distortions. The NASA Rotor 67 has been used as a baseline case in this study, while the boundary layer ingestion has been numerically simulated using an S-duct inlet. As a result, the combined modeling of the NASA Rotor 67 and the s-duct are capturing the flow fields typically experienced by the propulsion systems of future blended wing body aircraft concepts. Full annulus, steady-state, three-dimensional modeling has been used for the combined analysis of the rotor and s-duct. The NASA Rotor 67 computational fluid dynamics model is validated by the experimental data available in the open literature. Results indicated that the isentropic efficiency and pressure ratio have reduced by 7.08% and 7.19%, respectively due to the inlet distortions. The flow redistribution upstream of the fan causes a non-uniform work distribution across the complete fan face. A localized multi-objective design optimization featuring a surrogate model-based genetic algorithm setup was then applied to the transonic rotor tips. The optimized rotor design resulted in improved overall performance and relatively stable operation under the influence of inlet distortions compared to the baseline. The findings indicate an overall stable operation under the influence of the upstream distortions across the blade span rather than just an improved tip performance.

Keywords: NASA Rotor 67, s-duct, inlet distortions, numerical analysis, multi-objective genetic algorithm (MOGA), localized transonic tip optimization

Table of Contents

List of figures

List of Tables

List of Nomenclature

Symbols

C	Velocity, ms^{-1}
D	Diameter, m
M	Mach number, (-)
P	Pressure, Pa
T	Temperature, k
TR	Temperature ratio, (-)
U	Blade speed, ms^{-1}
ṁ	Mass flow rate, $kg.s^{-1}$
s	Entropy, J.$kg^{-1}K^{-1}$
t	Tip clearance, mm
x	Design input variables, (-)
y	Output response, (-)
α	Swirl angle, ^{o}
β	Air inflow angle/Regression coefficient, ^{o}/-
η	Isentropic efficiency, %
θ	Circumferential coordinate, ^{o}
π	Pressure ratio, (-)
ρ	Density, kgm^{-3}

Abbreviations

BWB	Blended wing body
CFD	Computational fluid dynamics
DOE	Design of experiment
LE	Leading-edge
MOGA	Multi-objective genetic algorithm
NS	Near stall
PE	Peak efficiency
RSA	Response surface approximation
TE	Trailing edge

BLI	Boundary layer ingestion
FSI	Fluid-structure interaction
DPS	Distributed propulsion system
PAI	Propulsion airframe integration
CFF	Cross flow fan
HWB	Hybrid wing body
STOL	Short take-off and landing
CESTOL	Cruise efficient short take-off and landing

Subscripts

1	Value at S-duct inlet
2	Value at fan face
a	Axial
b	Blade
f	Fan
l	Leading-edge
o	Stagnation quantity
r	Radial
t	Trailing edge
clr	Clearance
Mid	Mid span
Rel,t	Tip relative

Superscripts

-	The average or mean value

List of Publications

1. Parametric Optimization of NASA Rotor 67 Transonic Tips for Improved Localized Distortion Tolerance against Boundary Layer Ingesting Flows

   Aerospcae Science and Technology (Under Review)

   Authors: Talha Bin Tahir, Adeel Javed, Adnan Maqsood

Chapter 1

Introduction

1.1 Background

Worldwide, flights produced 915 million tons of CO_2 in 2019[1]. These emissions have devastating effects on the climate. European Commission adopted a series of legislative proposals setting it how to achieve the target of a net reduction of 55% in greenhouse gas emissions by 2030. Various technologies are used to reduce the overall fuel consumption in modern commercial aircraft. One such technology is the use of blended wing body aircraft (BWB). These aircraft have the potential to theoretically reduce the overall fuel consumption by 15%[2], [3]. Aside from fuel consumption, noise is becoming increasingly important in the commercial engine industry as regulations tighten. Increased noise pollution can lead to airport curfews, which raises overall operational costs due to reduced airport capacity in a given time. When it comes to engine design, factors such as fuel consumption, emissions, noise, drag, and weight all play a significant role in overall aircraft performance. Propulsion airframe integration (PAI) is another critical component in achieving future aviation goals.

Because of the increased aerodynamic efficiency over conventional airframe design, hybrid wing bodies have grown in popularity. The line between fuselage and wings is blurred in this configuration. One such configuration is the Blended Wing Body (BWB), in which the propulsion system is mounted on the upper aft surface of the fuselage. PAI can be achieved on a BWB by podding the engines or embedding them into the aft fuselage section as shown in fig. 1. While podded engines benefit from uniform flow into the engine, this concept is associated with increased structural mass, drag, and, as a result, increased fuel consumption. The ingestion of the boundary layer is implied by embedding the engines in the fuselage. As a result of the reduced momentum deficit, this concept has been shown to provide a reduction in overall fuel burn. An aircraft's momentum wake contains both lift-induced and viscous contributors. While the lift-induced component is fixed, the viscous component can be reduced through boundary layer ingestion. The

propulsion system re-energizes the low momentum fuselage boundary layer before it exits into the atmosphere thus increasing the propulsion efficiency[4]. As a result, the entire momentum wake deficit of the aircraft is reduced, as is the total drag of the aircraft. Because of BLI, the inlet has a lower mass averaged stagnation pressure. This results in an overall loss to the engine's thermodynamic cycle as well as increased viscous losses. The use of a distributed propulsion system over the aft fuselage is another concept associated with boundary layer ingestion in BWB. Kok et al.[5] demonstrated that a three-engine configuration resulted in a 5% reduction in fuel consumption for a 2% increase in pressure loss. It was also found that the potential of BLI is greater for larger engines than

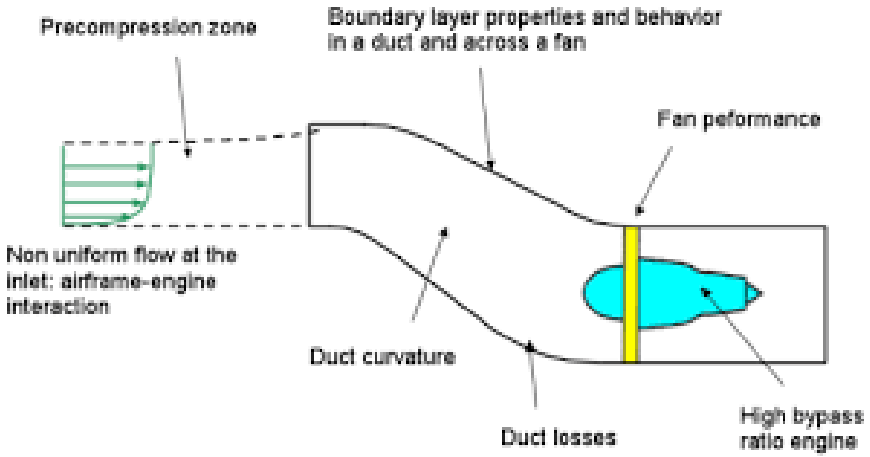

Figure 1.1: Embedded engine configuration ingesting boundary layer

for smaller engines, as the latter suffer from high-efficiency losses due to the scale effect, which outweighs the benefits of BLI. To maximize engine performance while taking advantage of the reduced momentum deficit, a careful selection of the number of engines as well as the proper design of the fan blade are required.

1.2 Research gap

As shown in fig 1, the boundary layer is ingested by the fan and therefore high fidelity CFD simulations are required to accurately capture this phenomenon. The most up-to-date research is present using a low-pressure sector with a specified sector angle and used as an inlet condition to generate the distorted upstream flow condition. This upstream flow field is far from reality and is just used to understand the flow physics inside the blade passages for the fans operating in inflow distortions.

To accurately capture the development of the boundary layer and to understand the physics of the flow when ingested by the engines of the BWB aircraft, it is necessary to perform the simulation of the complete aircraft with the engines attached to the aft of the fuselage. A lot of research has been done in the past to understand the flow topography inside the blade channels when subjected to inlet distortion, but very little research is done on redesigning the fan that will perform with better performance and efficiency than the baseline fan. Ingesting the boundary layer not only reduces the fan performance but also has detrimental effects on the blade structure. The blades are continuously subjected to regions of high- and low-pressure region, generating fatigue in blades which can ultimately lead to blade failure. Thus, detailed fluid-structure interaction (FSI) simulations are required to design a blade that not only gives an improved aerodynamic performance but is also durable.

Another factor that needs attention is the noise signature generated by the transonic blade tips upon interaction with the upstream distorted flow field. The inlet distortion causes high-velocity fluctuations and increased rotor wakes to generate an increased level of noise which needs to be brought to an acceptable level.

One of the most important parameters for controlling the level of distortion reaching the fan is the design of the inlet duct. The BWB aircraft's design causes the engine to ingest the boundary layer, but the more the boundary layer is ingested, the worse the conditions for the fan. This requires careful design for the inlet duct to reduce the flow separation and secondary flows formed due to the curvature of the duct and achieve the highest-pressure recovery which is the ratio of the total pressure at the fan face to the upstream total pressure.

1.3 Aims and Objectives

The tip of the modern fans lies in the transonic regime and slight non-uniformities can lead to increased losses and can cause enhanced losses. Therefore, the focus is to understand the flow physics for the axial fan when subjected to inlet distortions coming from an S-duct attached to the axial fan that mimics the top surface of the BWB aircraft and to perform a local optimization at the blade tip for designing a distortion-tolerant fan.

ANSYS CFX is the tool to conduct the simulations on the model developed to achieve the above-mentioned objectives

The main objectives of this study are:

- Numerically model and simulate the s-duct and axial fan (rotor 67)
- study the internal blade passage flow topography
- DOE for three parameters at tip i.e., leading-edge angle, trailing-edge angle, and tip clearance
- tip optimization using surrogate model based MOGA
- Validation via CFD and detailed analysis
- comparison of baseline case with the optimized case

1.4 Present work

The chapters to follow are briefly described below:

Chapter 2 would cover the literature review of the most relevant research on inlet distortions and their effect on the fan performance and flow topography within the blade channels and methods employed to perform blade optimization using different mathematical and statistical tools

In Chapter 3, different computational numerical models for axial fan modeling would be overviewed to opt for suitable models to evaluate and simulate the flow topography and fan performance.

Chapter 4 would be dedicated to the detailed CFD methodology of the model. The implementation of RANS modeling with boundary conditions in CFX would be described. Further, the creation of the domain, the choice of turbulent model, setting up appropriate boundary conditions, the numerical discretization schemes, and other solver setups would be explained. The validation and verification of the numerical setup and the solution would be presented towards the end of this chapter.

Chapter 5 would present the results from the numerical simulations of both the baseline fan and the optimized fan. The results would be compared with those from the numerical modeling of the single passage rotor alone simulation with a clean inlet. This would bring

us to the conclusion of this research and hence a summary of major findings and further possibilities of research will be discussed.

Summary

This chapter describes the background of this thesis work. The BWB aircraft offer the potential to reduce emissions by improving fuel efficiency. The design of these aircraft helps to cut the excess fuel required to produce the same thrust to propel the aircraft by increasing the propulsive efficiency. The major drawback of this configuration is the reduced fan performance and increase aerodynamic losses. The boundary layer formed over the aircraft body is ingested by the aircraft. The non-uniform flow distribution upstream of the fan reduces the fan efficiency. This demands redesigning the fan for increased performance, structural durability, and reduced noise in the presence of inlet distortions.

References

[1] Hydrogen-powered aviation, no. May. 2020.

[2] S. Sato, “The Power Balance Method For Aerodynamic Performance Assessment,” Aeronaut. Eng. Massachusetts Inst. Technol., p. 207, 2012.

[3] C. Goldberg, D. Nalianda, D. MacManus, P. Pilidis, and J. Felder, “Method for simulating the performance of a boundary layer ingesting propulsion system at design and off-design,” Aerosp. Sci. Technol., vol. 78, pp. 312–319, 2018, doi: 10.1016/j.ast.2018.04.026.

[4] L. H. Smith, “Wake ingestion propulsion benefit,” J. Propuls. Power, vol. 9, no. 1, 1993, doi: 10.2514/3.11487.

[5] H. J. M. Kok, M. Voskuijl, and M. J. L. Van Tooren, “Distributed propulsion featuring boundary layer ingestion engines for the blended wing body subsonic transport,” 2010, doi: 10.2514/6.2010-3064.

Chapter 2

Literature Review

2.1 Types of Distributed Propulsion Systems

There are a lot of distributed propulsion configurations that have been proposed. Any aircraft that has more than one propulsion system can be categorized as distributed propulsion syst em (DPS). Two such configurations are shown in fig 2.

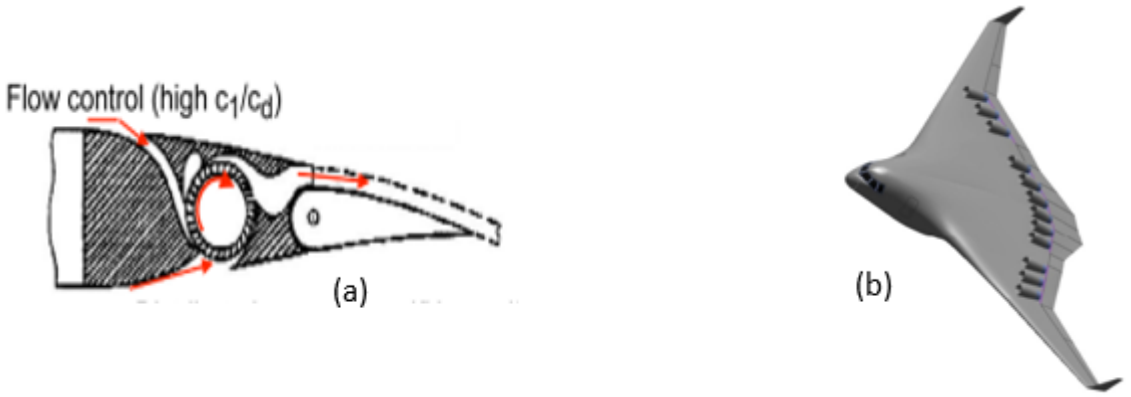

Figure 2.1: Configurations for distributed propulsion system (a) cross flow fan, (b) multiple discrete engines

Figure 2(a) shows a DPS integrated with a cross-flow fan (CFF), also called a transverse fan. This is a two-dimensional fan installed into the wing of the aircraft producing thrust along the wingspan. The fan uses the upper and lower surface boundary layer and ejects it near the trailing edge of the wing. Two gas generators installed on the wing root and tip transmits power to the CFF. However, this idea was never implemented due to low fan performance and the difficulty of installing CFF into the wing structure

Several aircraft with propulsors mounted on the front, aft, and within the wing have been flown. Although the number of propulsors required to classify the propulsion system as DPS is not clearly defined. YB-49 is an example with four turbojet engines installed on either side of the wing with rectangular inlets and circular nozzles. A new hybrid wing body (HWB) also called blended wing body (BWB) aircraft is proposed to achieve high cruise efficiency, lower noise signature, and large internal volume to integrate the

propulsors [1]. It is a cruise-efficient short take-off and landing (CESTOL) aircraft as shown in fig 2(b). The propulsion system is based on 12 small conventional engines to enable short take-off and landing (STOL) installed on the upper body of the aircraft near the trailing edge

2.2 Classification of inlet distortions

There are a lot of different kinds of distortions based on the effect, pattern, motion state, or duration time. As for the effect of the inlet distortion on the rotor flow field, inlet distortions are categorized into total pressure distortion, total temperature distortion, and swirl distortion. Depending upon the pattern of the inlet distortions they can be categorized as radial distortions and circumferential distortions. As for the state of the motion, distortions can be categorized as stationary distortion and rotating distortion. Depending on the duration time, inlet distortions can be categorized as consistent distortion and abrupt distortion. Usually, the inlet distortion is highly complex and a combination of different types of distortions and can change the compressor performance differently.

Usually, most of the research in the past has been done on stationary, consistent total pressure, and swirl distortion. The detailed literature on how different distortions affect fan performance is described later.

2.2.1 Total pressure distortion

Aircraft frequently encounter total pressure distortion ahead of the engine inlet during flight. This distortion can be due to the flow separation, boundary layer ingestion, ground vortex ingestion, and strong cross winds. Total pressure distortion affects the stability margin by reducing it. The efficiency of the rotor is reduced due to the mass flow distortion at the engine inlet which ultimately leads to an off-design incidence angle. Some experimental studies have been performed to understand the flow characteristics and overall fan performance in the presence of total pressure distortion[1].

2.2.2 Total temperature distortion

Total temperature distortion is caused due to vertical take-off, thrust reverser exhaust ingestion, weapon hot gas ingestion, steam ingestion during catapult launch from the aircraft carrier. The overall effect of total temperature distortion is nearly the same as that of total pressure distortion, reducing the stall margin and the efficiency of the rotor. In the

presence of the total pressure distortion, the compressor tends to attenuate it but it amplifies the total temperature distortion[2]. These distortions affect the stability of the downstream components such as the combustion chamber.

2.2.3 Swirl distortion

Swirl distortion can be caused due to the upstream flow redistribution, strong cross wind, and ground vortex ingestion. Depending on the rotation of the vortex relative to the rotor rotation, they are categorized into two main categories: (a) Bulk swirl, (b) paired swirl. Bulk swirl consists of a single vortex rotating in the direction of the rotor (co-swirl) or opposite to the rotor rotation (counter-swirl). Paired swirl consists of two vortices rotating in the opposite direction

2.2 Rotor-distortion interaction

2.2.1 Structural and noise signature analysis

As the boundary layer approaches the engine face, the fan is subjected to a non-axisymmetric total pressure profile. This reduces the fan total pressure ratio, efficiency and causes a loss in the stability margin. As the fan is continuously passing through sectors of low and high pressure, this results in unequal distribution of force on the blade. The continuous loading and unloading create fatigue and can cause severe damage to the blade. Another problem that attracts a lot of attention in the design of aircraft engines is the noise signature. Romani et al.[3] performed analysis on NOVA boundary layer ingestion configuration to check the variation in broadband and tonal fan noise when subjected to BLI. It was found out that BLI causes highly unsteady fan blade loading, rotor wake tangential velocity fluctuations, and high-velocity fluctuations. All these resulted in an overall increase of noise levels up to 18 EPNDB.

Bakhle et al.[4] performed flutter analysis for rotor at different rotational speeds for inlet distortions. The energy method was used to calculate the aerodynamic damping, the work done on the blade by unsteady pressure due to blade vibration. Results indicated that no flutter was indicated for the first three vibrational modes at all the rotational speeds. The aerodynamic damping was also positive at all times.

2.2.2 Internal flow topography and fan performance

Naseri et al.[5] studied the effect of radial total pressure and swirl distortion. Results indicate that hub and co-swirl distortions improve the stability margin while tip and counter-swirl deteriorate it. Another study performed by Verma et al. [6]shows that if the intensity of hub distortion is increased to a certain point, the stall margin is reduced but with tip distortion this reduction was comparatively lower. Fidalgo et al. [2]studied the fan performance for inlet distortion and compared the results with the experimental data. Results indicate that the inlet distortion reduces the fan efficiency without any significant reduction in the total pressure ratio. It was also found out that the mass flow excursions are reduced as the flow approaches the fan, but the swirl non-uniformities are intensified which leads to non-uniform work distribution across the fan face. The total pressure distortion upstream of the rotor alters the stability margin by reducing the choke mass flow rate[4]. This reduction depends on the intensity of the total pressure distortion. Zhang et al. [7]studied the effect of inlet distortion on the stability margin. The difficult flow structure near stall requires high temporal resolution to accurately determine the flow structure near stall. Results show that the stall margin loss is highly dependent on the fan rotational speed. As the rotational speed increases stall margin loss decreases but the total pressure loss increases

Hall et al.[8] performed a detailed analysis on the effect of different turbomachinery aspects on the rotor flow field in the presence of inlet distortions. Results indicate that the rotor has a reduced non-uniformity in flow field for non-axisymmetric stator geometry, increased stage flow, and stagnation enthalpy rise that may offer a potential for mitigating the reduced fan performance due to the presence of the inlet distortions.

Another factor affecting the stability margin is the internal blade passage losses caused by shock wave boundary layer interaction. In transonic compressors, due to high Mach numbers at the tip, diffusion is caused by the presence of the shock wave. This shock also comes with a disadvantage where it interacts with the blade boundary layer and causes it to separate from the blade surface. This low momentum boundary layer when mixed with the mainstream flow, causes mixing losses, and reduces the fan performance. Hah et al. [9] showed that at higher rotational speeds the shock wave interacts with the blade boundary layer, causing blockage and reducing stability margin. This interaction reduced

the blade efficiency near the tip region as compared to the near hub. It was also found out that at lower rotational speeds the blade showed an improved efficiency near the tip region. A detailed analysis of the loss sources in the BLI and fan interaction is performed by Gunn et al.[10]. The CFD results made a good agreement with the experimental data performed for the low-speed BLI rig fan. Another CFD simulation for the VITAL transonic fan was performed to study the shock structure. It was found out that the shock intensity, size, and position vary around the annulus. This led to the shock-boundary layer interaction and separation losses. The VITAL fan shows a less severe response at the tip than the rig fan due to smaller tip clearance than the rig fan.

Gunn et al. [1] experimentally evaluated the reduction in fan performance in the presence of the inlet distortion. Results show a reduction in fan total to the total efficiency of 5.3%. The reduction in rotor performance is dominated by the presence of an off-design incidence angle at the leading-edge (LE) across the whole fan face. The rotor does not remove the distortion which then proceeds to the stator where the off-design whirl angle from the rotor trailing-edge (TE) causes flow separation in stator rows.

2.3 Blade optimization

The BLI reduces the fan performance in which the efficiency of the fan suffers the most. Tip clearance is a sensitive parameter in terms of fan performance and stability margin. Thus, to improve the fan efficiency, a distortion tolerant fan must be designed that can efficiently work in these conditions. In general optimization of transonic fans has been done to improve the aerodynamic stability and improve the fan efficiency or pressure ratio. Sang-Bum Ma et al.[11] optimized the blade of a transonic fan using a surrogate-based multi-objective genetic algorithm (MOGA). Latin hypercube sampling is used to fill the design space for the input parameters. To account for the non-linearities in the objective functions, the response surface approximation (RSA) model was used. Results indicate an improvement of 17.2% in the stall margin at 60 % of the design rotational speed and a 2.96 % rise in efficiency. Benini et al.[12] optimized the rotor 37 using MOGA. A total of 23 parameters were used including 14 points for the camber line and 9 points for thickness distribution. A non-dimensional mass flow rate of 0.98 is used to simulate all the design space. From the Pareto front, two designs were evaluated, one with maximum efficiency and one with maximum pressure ratio. An improvement of 1.5% in efficiency

is observed without any change in the pressure ratio. The second design from the Pareto showed a slightly higher improvement in pressure ratio of 5.5 % with a 0.8% reduction in efficiency

Summary

This chapter provides a summary of the literature available on boundary layer ingestion. Different configurations of propulsion system integration are also described. The aircraft's inlet is always subjected to different types of distortions with different intensities which leads to reducing the pressure ratio, efficiency, and stall margin. Depending on the intensity of the inlet distortion, stresses and fatigue can lead to blade failure. These distortions also affect the noise signature of the boundary layer ingesting propulsion systems. These parameters can be improved by carefully redesigning the fan of the propulsion systems using different optimization techniques.

References

[1] E. J. Gunn, S. E. Tooze, C. A. Hall, and Y. Colin, "An experimental study of loss sources in a fan operating with continuous inlet stagnation pressure distortion," J. Turbomach., vol. 135, no. 3, 2013, doi: 10.1115/1.4007835.

[2] V. J. Fidalgo, C. A. Hall, and Y. Colin, "A Study of Fan-Distortion Interaction Within the NASA Rotor 67 Transonic Stage," J. Turbomach., vol. 134, no. 5, pp. 1–12, 2012, doi: 10.1115/1.4003850.

[3] G. Romani, Q. Ye, F. Avallone, D. Ragni, and D. Casalino, "Numerical analysis of fan noise for the NOVA boundary-layer ingestion configuration," Aerosp. Sci. Technol., vol. 96, p. 105532, 2020, doi: 10.1016/j.ast.2019.105532.

[4] M. A. Bakhle et al., "Aeromechanics analysis of a distortion-tolerant fan with boundary layer ingestion," AIAA Aerosp. Sci. Meet. 2018, no. 210059, pp. 1–18, 2018, doi: 10.2514/6.2018-1891.

[5] A. Naseri, M. Boroomand, and S. Sammak, "Numerical investigation of effect of inlet swirl and total-pressure distortion on performance and stability of an axial transonic compressor," J. Therm. Sci., vol. 25, no. 6, pp. 501–510, 2016, doi: 10.1007/s11630-016-0891-6.

[6] V. Verma, G. Singh, and A. M. Pradeep, "The effect of inlet distortion on low bypass ratio turbofan engines," Proc. Inst. Mech. Eng. Part G J. Aerosp. Eng., vol. 234, no. 8, pp. 1395–1413, 2020, doi: 10.1177/0954410020909190.

[7] W. Zhang, S. Stapelfeldt, and M. Vahdati, "Influence of the inlet distortion on fan stall margin at different rotational speeds," Aerosp. Sci. Technol., vol. 98, p. 105668, 2020, doi: 10.1016/j.ast.2019.105668.

[8] D. K. Hall, E. M. Greitzer, and C. S. Tan, "Analysis of fan stage conceptual design attributes for boundary layer ingestion," J. Turbomach., vol. 139, no. 7, 2017, doi: 10.1115/1.4035631.

[9] C. Hah, D. C. Rabe, T. J. Sullivan, and A. R. Wadia, "Effects of inlet distortion on the flow field in a transonic compressor rotor," ASME 1996 Int. Gas Turbine

Aeroengine Congr. Exhib. GT 1996, vol. 1, no. April 1998, pp. 233–246, 1996, doi: 10.1115/96-GT-547.

[10] E. J. Gunn and C. A. Hall, "Aerodynamics of boundary layer ingesting fans," Proc. ASME Turbo Expo, vol. 1A, pp. 1–13, 2014, doi: 10.1115/GT2014-26142.

[11] S. B. Ma, A. Afzal, K. Y. Kim, J. Choi, and W. Lee, "Optimization of a two-stage transonic axial fan to enhance aerodynamic stability," Proc. ASME Turbo Expo, vol. 2C-2016, no. June, 2016, doi: 10.1115/GT2016-56261.

[12] E. Benini, "Three-dimensional multi-objective design optimization of a transonic compressor rotor," J. Propuls. Power, vol. 20, no. 3, pp. 559–565, 2004, doi: 10.2514/1.2703.

Chapter 3

Axial fans numerical modeling methods

3.1 Analytical and numerical methods

Based on the findings from the experimental data of the axial fans under inlet distortions, several numerical methods and techniques have been devised to predict the fan performance under the influence of inlet distortions. These methods can provide sufficient information about the basic fan behavior for inlet distortions and are relatively less expensive and time-consuming as compared to the experimental setups. With the rapid growth of computational methods and algorithms, computational fluid dynamics is becoming more accurate to predict the fan performance and stability performance with relatively high accuracy. Considering that the detailed flow measurements are still very hard to achieve especially in a rotating domain. Furthermore, in the presence of the inlet distortions, the extreme blade vibrations and rotating stall can damage the test rig. In these cases, CFD simulations have an upper hand in which highly complex 3D flows can be accurately captured without the need for an expensive and time-consuming experimental setup.

There are several different numerical methods employed to study the fan performance under the influence of inlet distortions:

3.1.1 Parallel compressor method

First proposed in 1959 by Pearson et al.[1], the parallel compressor method is a widely used technique for determining the fan performance under the influence of inlet distortions. Although the theory has some oversimplifications, it is a useful method for qualitative analysis for fans operating in inlet distortions. The basic methodology of the parallel compressor method is shown in fig 3. The compressor subjected to inlet distortion can be divided into two separate sectors, one with the clean inlet and the other with the distorted inlet. The overall performance can be taken as the average of both sectors. The three assumptions that must be satisfied are:

1. The pressure ratio and mass flow of both the sectors lie on the same clean flow characteristic line.
2. Since both the sectors are discharging into the same plenum, the exit static pressure is the same
3. No circumferential flow transfer takes place between two sectors.

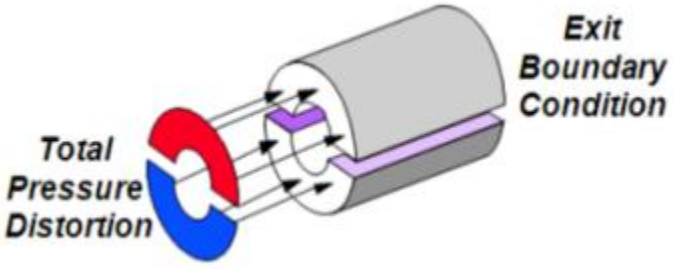

Figure 3.1: Parallel compressor methodology for inlet distortions

3.1.2 Actuator disk model

The actuator disk model takes each blade as a discontinuity in the flow field while the streamlines and the mass flux are continuous. The blade row is reduced to zero thickness and all the loading is concentrated in the plane. Combined with the inlet and outlet boundary conditions, the generic equations that describe the flow across the disk can be solved. Since the plane has zero thickness and no blade chord is considered, the actuator disk model fails to solve the flow features inside the blade passages, choke mass flow, shock wave positions, and other flow characteristics related to the blade geometry. The Semi-actuator disk model, on the other hand, models the rotor as a one-dimensional channel of finite axial length and hence is able the calculate the inside blade channel flow field. Some improved models of actuator disk model can also be found as proposed by Ref.[2].

3.1.3 Body force method

The two-body force methods include the bulk body force method and viscous body force method. The bulk body force method models the compressor with a simple duct neglecting the geometry of the blade. The blade force and the viscous terms are modeled in the Euler equations. The second methods consider the blade geometry and solve the Euler equations while considering the viscous terms. In this method, a relatively coarse mesh and larger

time step can be used that will significantly reduce the computational cost as compared to the URANS.

The body force method uses two simplifications: the blades are infinite, and the localized pressure rise in the blade passage can be defined. Incompressible Euler equations are used to solve the flow in ducts and gaps. Based on the infinite blades assumption, the flow can be treated as axisymmetric at each circumferential position in a coordinate frame fixed to the blade row. A body force field is introduced to simulate the pressure rise and flow turning due to the blades.

3.1.4 URANS

The flow field in the rotor is highly unsteady and three-dimensional. The analytical methods and body force method however can predict the overall performance of the rotor with good accuracy but due to some simplifications and assumptions, the highly complex flow field inside the blade passages cannot be accurately captured. In addition, the body force for low mass flow conditions in the distorted region might be impossible to obtain from clean flow conditions and hence body force method is applicable away from the stall in the presence of inlet distortions. With the soar of computational capability, high fidelity simulations like URANS and large eddy simulation (LES) are developed to capture the flow field for inlet distortions. URANS have proved its capability to model the complex unsteady phenomenon like rotating stall and surge of multi-stage compressor[3].

Summary

This chapter summarizes the available numerical and analytical methods that can be used to predict the overall rotor performance. Each model due to its oversimplifications fails to predict the flow field in the blade channel but can determine the overall fan performance with good accuracy in the presence of inlet distortions. Some models have been improved over time and provide a better understanding but still lack to accurately capture the highly complex 3D flow field in the rotor, especially rotating stall and surging in compressors. In this matter, URANS has an upper hand in providing a detailed understanding of the flow field in the presence of inlet distortions and is also a proven technology by literature.

References

[1] J. Gunkelman, “Technical notes,” J. Neurother., vol. 6, no. 2, p. 45, 2002, doi: 10.1300/J184v06n02_06.

[2] W. G. Joo and T. P. Hynes, “The simulation of turbomachinery blade rows in asymmetric flow using actuator disks,” J. Turbomach., vol. 119, no. 4, 1997, doi: 10.1115/1.2841182.

[3] J. Dodds and M. Vahdati, “Rotating stall observations in a high speed compressor-part II: Numerical study,” J. Turbomach., vol. 137, no. 5, 2015, doi: 10.1115/1.4028558.

Chapter 4

Implementation of CFD for Axial fan for inlet distortions

4.1 Outline of the study

The methodology used for this study is shown in fig 4. The analysis is performed in ANSYS CFX. The numerical code used for the study of fan-inlet distortion interaction is validated against the experimental data. The second step involves using the code to model the rotor in the presence of inlet distortions. The third step is to determine the fan performance and analyze the rotor flow field for inlet distortions. The next step is to perform localized tip optimization to enhance the rotor performance and improve the rotor flow field. The final step is to compare the optimized rotor with the baseline rotor.

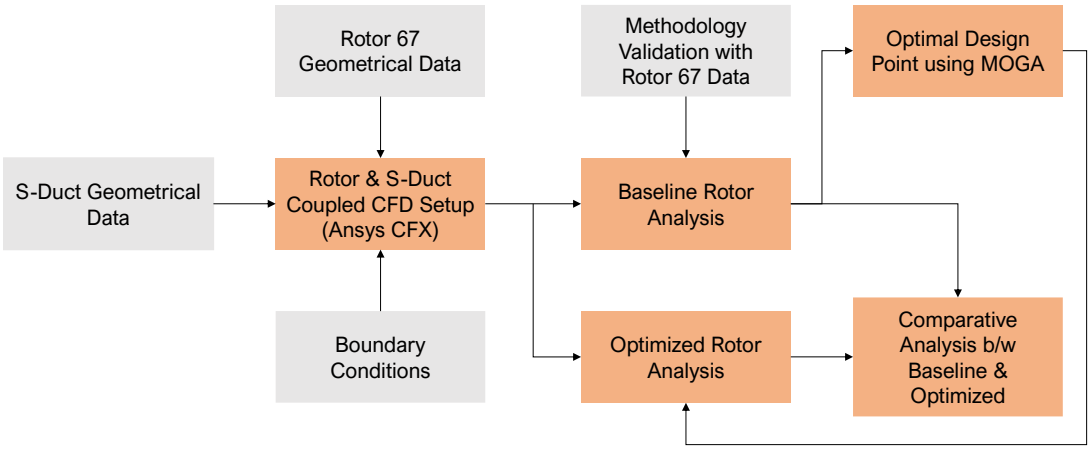

Figure 4.1: Methodology used for design and analysis of axial fan in the presence of inlet distortion

4.2 Case study

The case study is divided into two parts: (a) Modelling of baseline fan in the presence of inlet distortions, (b) Modelling of optimized fan in the presence of inlet distortions. An applied methodology has been used to model the axial fan and the S-duct using computational fluid dynamics (CFD). The axial fan used for this study is NASA rotor 67. The rotor is designed by using the coordinates obtained by NASA[1]. The experimental data for the total pressure ratio, efficiency, and blade to blade contours are used to validate the CFD model. The design of the s-duct is based on the prototype of inlet A[2]. The geometric parameters for rotor 67 and s-duct are shown in fig 5.

Parameters	Rotor
Number of blades, (-)	22
Rotational speed, min^{-1}	16043
Tip clearance, t_{clr} (mm)	1.016
Tip relative Mach number, $M_{rel,t}$ (-)	1.38
Design fan pressure ratio, π_f, (-)	1.63
Design point isentropic efficiency, η (%)	92
Rotor Diameter, D (m)	0.51

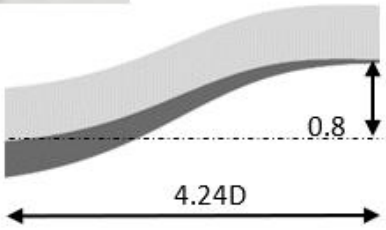

Figure 4.2: Geometric parameters for NASA rotor 67 and s-duct

4.3 CFD setup

4.3.1 Baseline case

4.3.1.1 Computational domain and boundary conditions

Figure 6 shows the computational domain for the NASA rotor 67 with a clean inlet case and with s-duct. First, a single passage domain is simulated which acts as a clean inlet case in which no inlet distortions are considered. This case is then validated against the experimental data available for NASA rotor 67 with a clean inlet[1]. At the inlet, total temperature, total pressure, and inlet swirl flow angles are specified. For the clean inlet flow, circumferential flow angles are kept zero, and flow is considered normal to the boundary. The turbulent intensity of 5% is used as suggested by CFX. The RNG k-e turbulence model is used with scalable wall functions. The rotor shroud is defined as counter-rotating. The mixing plane is used as an interface between the rotor, inlet, and outlet. It does circumferential averaging of velocity, pressure, and turbulence variables upstream of the interface and uses them as input variables downstream of the interface. The lateral sides of the blade passage are treated as periodic boundaries. The outlet static pressure boundary condition is used to generate the compressor map. The choke mass flow is calculated and then the static pressure is gradually increased until the point where the solver crashes. This indicates the stall.

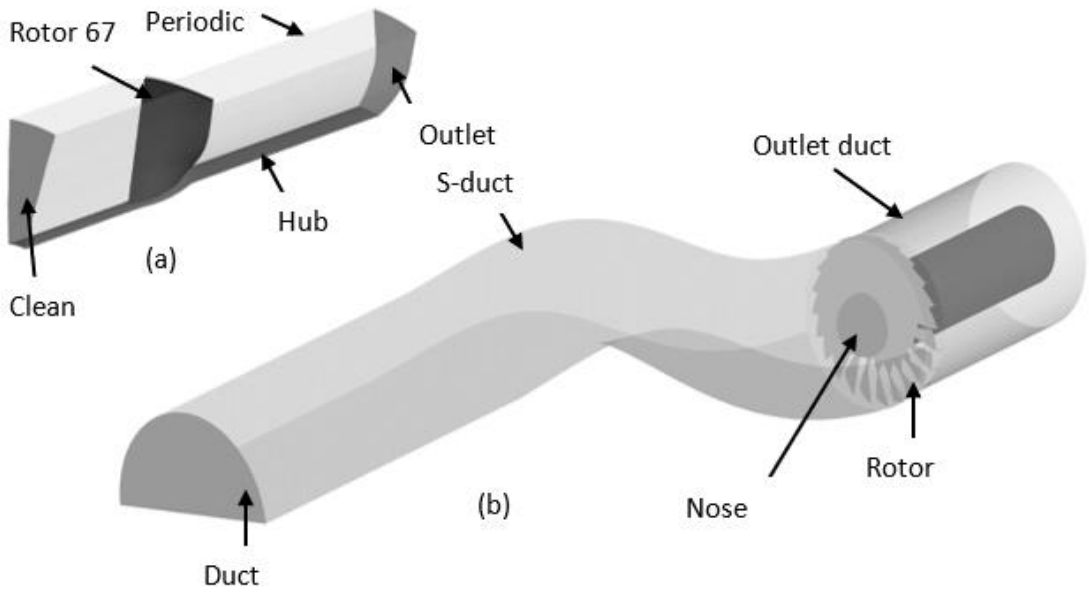

Figure 4.3: Computational Domain of (a) NASA rotor 67 for clean inlet, (b) NASA rotor 67 with S-duct

For the BLI study, steady-state, full fan annulus is considered rather than the single passage to accurately model the circumferential distortions. The S-duct is attached to the fan inlet by a frozen rotor interface which transfers the circumferential distortion across the interface without doing the circumferential averaging done by the mixing plane. The fan inlet, rotor domain, and outlet are also connected by a frozen rotor interface. For the whole annulus modeling, the lateral surfaces of the blade passages are connected by general connection. The blade tip and the shroud casing are connected by general connection. To let the boundary layer grow and capture the actual flow field, the length of the duct has been increased by nearly 3.8D. The fan inlet is shortened to reduce the distance between the rotor inlet and duct outlet. The outlet has been increased by 1.5D to let the flow develop and help in convergence. The total pressure, total temperature, and swirl angles are defined at the duct inlet. The base of the duct is treated as a wall to mimic the upper surface of the aircraft. The top surface is treated as a free wall to avoid the boundary layer growth due to wall friction.

The s-duct is designed using solid works while the rotor is designed in ANSYS bladegen modeler. The coordinates used for the design of the rotor are the axial distance (Z), radial distance (R), thickness distribution, and beta (β). The axial and radial distance is used to define the blade geometry and flow path. Beta defines the angle of the mean camber line from the meridional direction while thickness is the normal distance from the mean camber line to the blade surface. These four coordinates combined in bladegen helps in designing the rotor which is then exported to turbogrid for blade meshing.

4.3.1.2 Grid processing and sensitivity analysis

The blade geometry constructed in bladegen is exported to ANSYS TurboGrid for meshing. It is software vastly used in turbomachinery applications. H-Grid and O-Grid topology is used to mesh the inlet, outlet, and blade passage. The O-Grid is used for meshing the blade while the rest of the domain is meshed using the H-Grid topology. Tip clearance is introduced by trimming down the blade tip. The S-duct is meshed using the ANSYS meshing tool. Inflation is used on the flat surface of the duct to accurately model the boundary layer growth. Scalable wall functions are used to make a compromise between computational cost and accuracy. The y^+ used lies in the range of $10 < y^+ < 65$. Four grids of sizes 0.11 million, 0.32 million, 0.90 million, and 2.8 million were used. The

output variables are fan pressure ratio and efficiency. The maximum difference in pressure ratio and efficiency was found out to be 2.8% and 1.84%. The analysis shows convergence at around 0.9 million (0.68 million for the rotor). Consequently, the whole domain consists of around 23.46 million elements comprising 2.8 million elements in the S-duct and 20.46 million elements in the fan domain with 3.65 million elements in the fan outlet.

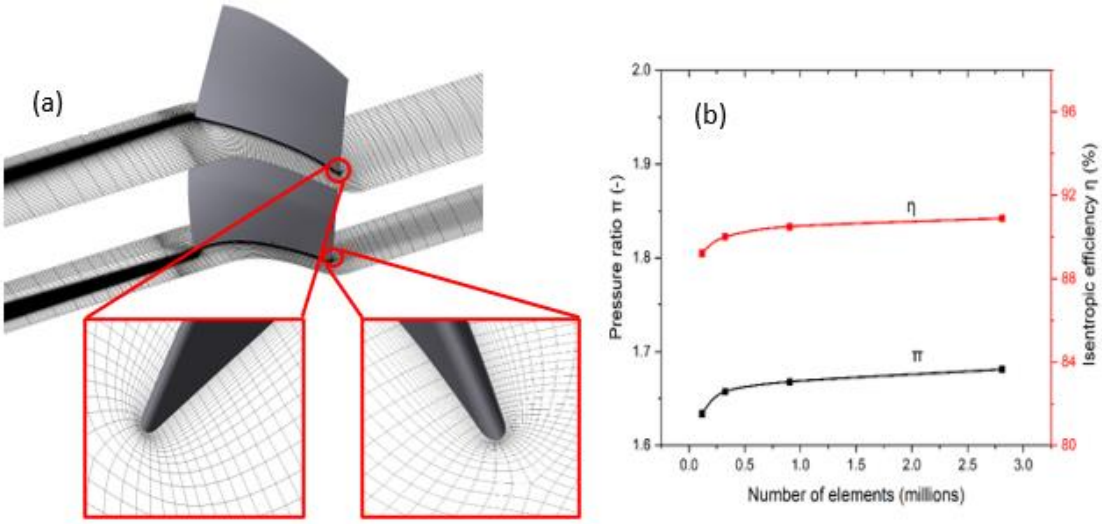

Figure 4.4: (a) Rotor grid at mid span and hub and (b) mesh independence study

4.3.1.3 Solver setup

The numerical setup for modeling the axial fan required a high-resolution advection scheme and turbulence numerics. The convergence control setup was set to an auto timescale with a factor of 1. The value of the timescale factor was gradually increased near the stall point to achieve convergence and reduce the computational time required. The value of RMS for residuals used was 1E-04. The iterations were continued until continuity residuals dropped below 1E-04 while the other residuals dropped below 1E-03. But the residuals were not the only deciding factor for terminating the simulations. Monitor points for mass in, mass out, pressure ratio, and efficiency were also monitored. The iterations were terminated when the monitor points became steady, and no significant variation was observed in the value.

4.3.2 Optimized case

The second part of the case study includes redesigning the rotor with better performance than the baseline case in the presence of inlet distortions. This is done by performing a localized tip optimization. The tips of the transonic fans are sensitive regions and are prone to inlet variations. Any significant changes upstream of the fan near the tips can significantly reduce the fan performance. The computational domain, solver setup, and grid for both the baseline and the optimized case are the same. The only difference is the rotor. A multi-objective technique has been used for the local tip optimization. Two objective functions are defined to optimize the pressure ratio and isentropic efficiency of the fan. The fan efficiency is the primary objective function that needs to be maximized. Figure 8 shows the detailed methodology applied for the design of the optimized rotor.

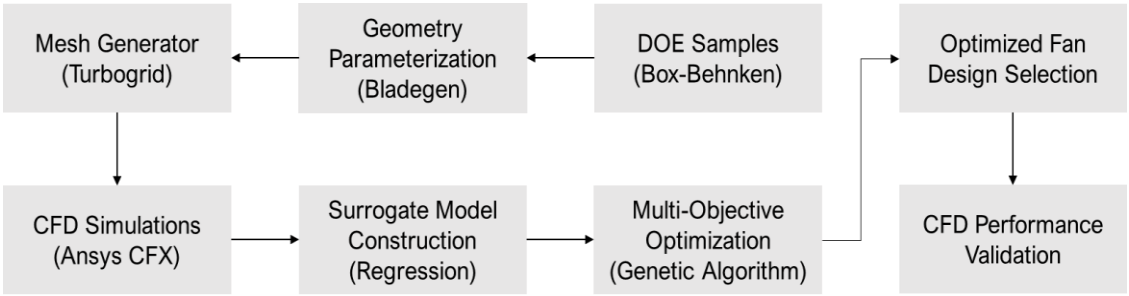

Figure 4.5: Flow chart for fan design optimization methodology for inlet distortions

4.3.2.1 Box Behnken Design (BBD)

The first step is to create a design of experiment (DOE) for the selected variables. DOE is a method used to determine the effect of the system input variables on the performance and output response variables. These DOE samples are used to design a surrogate model later used for optimization. The accuracy of this model is highly dependent on the number of DOE samples. The more the sample size the more the accuracy of the model. But increasing the sample size also increases the computational cost which negates the benefits of the surrogate model. To reduce the computational cost, the box Behnken method for DOE is used. BBD partitions the design space by assigning the variable three values at the minima, maxima, and the mid-point of the design space. Three variables used for BBD are the tip leading edge angle, trailing edge angle, and tip clearance. The design space is given in table 1.

Table 4.1: Design Space

Input Variable	Nominal Value	Range
LE blade angle, $\beta_{b,l}$ (°)	65.83	±2.5
TE blade angle, $\beta_{b,t}$ (°)	54.42	±2.5
Tip clearance, t_{clr} (mm)	1.016	±0.5

4.3.2.2 Surrogate model

A surrogate model is based on the data obtained by high-fidelity CFD simulations using the DOE samples. The model can help to predict the response variables using a mathematical model instead of using time-consuming CFD simulations. The accuracy of the model is checked using the value of R^2. Higher the value of R^2, the better the surrogate. A lot of surrogate models are available including polynomial response surface, kriging, gradient enhanced kriging, and artificial neural network, etc. The response surface methodology is used for this study.

RSM is used to fit the CFD simulation database obtained from the DOE samples. It uses a second-order polynomial having intercept, linear, product, and square terms. This helps in predicting the relationship of the input variables with the output response variables. The response surface equation in generic form is given as:

$$y = \beta_o + \sum_{i=1}^{n} \beta_i x_i + \sum\sum_{i<j} \beta_{ij} x_i x_j + \sum_{i=1}^{n} \beta_{ii} x_i^2 + \varepsilon$$

where β, x and n represents the regression coefficient, design variable, total number of design variable. As the study includes two objective functions, two separate meta-models were created. The first metamodel was created for isentropic efficiency to fit the CFD simulation data. The value of R^2 and adjusted R^2 is 0.9924 and 0.9786 respectively. This shows the ability of the surrogate to predict the isentropic efficiency with very high accuracy without the need for high fidelity CFD simulation. The second metamodel was created for pressure ratio. The value of R^2 and adjusted R^2 is 0.9915 and 0.9762 respectively. These metamodels are further used for optimization. A sensitivity analysis was performed to determine to which variables the objective functions are more sensitive. It can be seen in fig. 9 that the isentropic efficiency is more sensitive to the tip clearance

as compared to the leading and trailing edge angle. The efficiency is the least sensitive to the trailing edge angle as can be seen from the individual variable terms. The pressure ratio is sensitive to the tip clearance and the blade leading edge angle as it plays an important role in the incidence angle.

4.3.2.3 Multi-Objective optimization

MATLAB optimization tool has been used for multi-objective design optimization. Several optimization algorithms are available including least square, mixed-integer linear programming, and genetic algorithm along with multi-objective genetic algorithm. The aim of the study includes two objective functions: isentropic efficiency and pressure ratio.

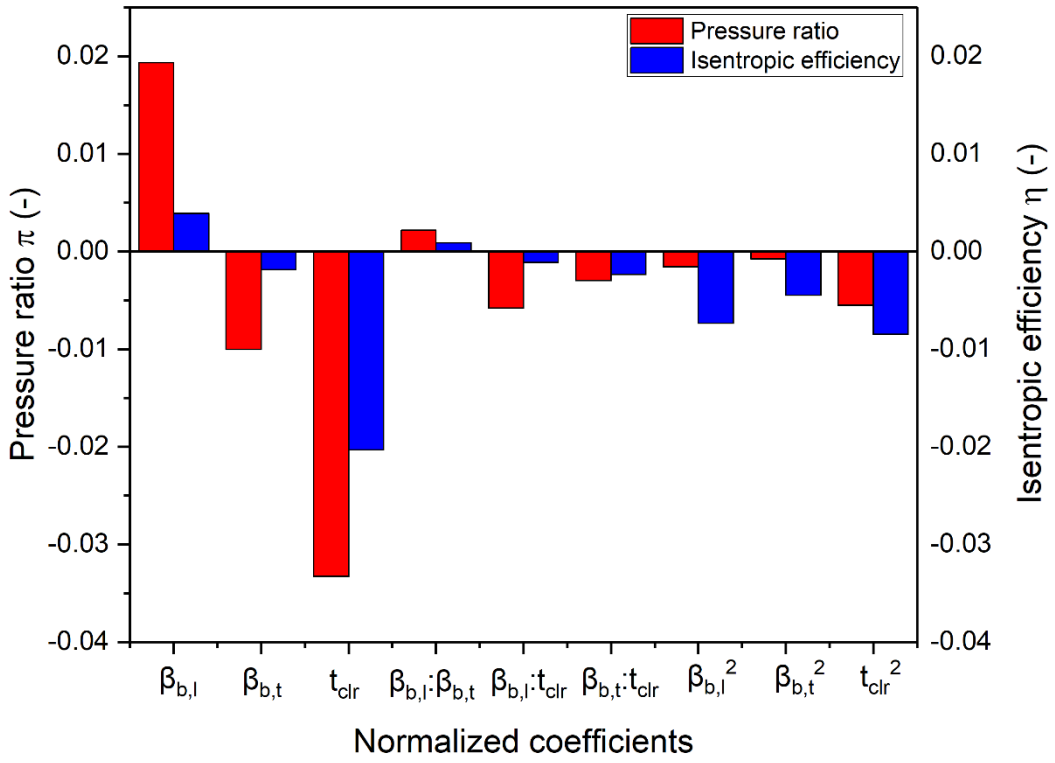

Figure 4.6: Sensitivity analysis of objective functions for input parameters

Therefore, a multi-objective genetic algorithm is used. The natural selection process mimicking the biological evolution process is used to find the set of non-dominated solutions called the Pareto front. These are the optimal solutions in which to improve one objective function, the other objective function gets sacrificed. The goal was to determine these Pareto points and quantify the tradeoffs to satisfy the major objective of increasing efficiency. These Pareto points as shown in fig. 10 are obtained from a multi-objective

genetic algorithm by using a population size of 100 with 100 generations. The population size specifies that how many individuals are in a generation while generations represent the number of iterations. The size of 2 is used for the tournament as proposed by Ref.[3], which selects each parent by choosing individuals at random. The crossover production size of 0.8 is used as proposed by Ref.[3], which determines how the genetic algorithm produces children at each new generation. The design point with the highest efficiency is used for the optimized fan which suggests using a lower tip clearance value and slightly higher value for leading and trailing-edge angle as compared to the baseline fan. These new values for the three variables are then updated in the CFD model and the results show a good match between the CFD data with that predicted by the surrogate model as can be seen in table 2.

Table 4.2: Percentage difference between surrogate model and CFD

Objective functions	Surrogate model	CFD	Percentage difference (%)
Pressure ratio π (-)	1.515	1.5157	+0.046
Isentropic efficiency η (-)	0.84395	0.84052	-0.407

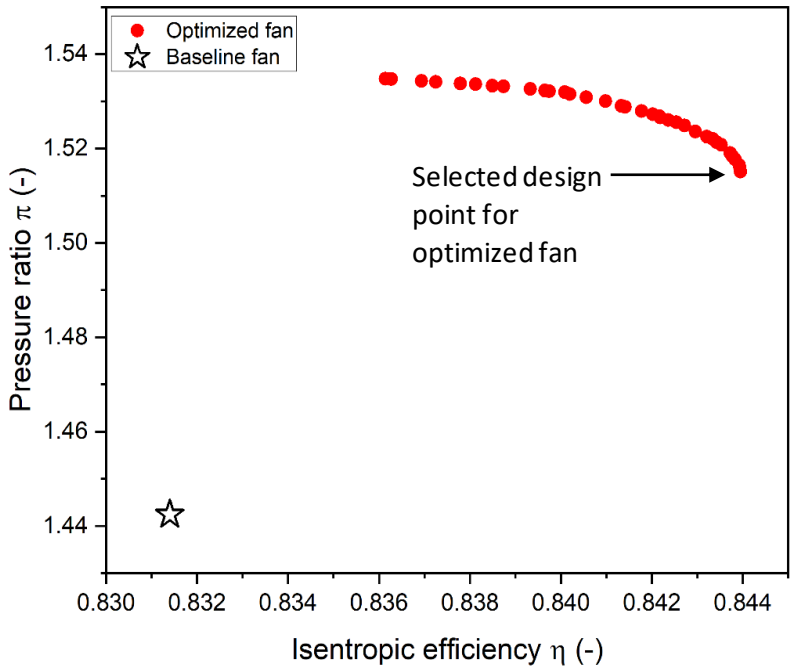

Figure 4.7: Pareto front for pressure ratio and isentropic efficiency

Summary

This chapter described the methodology applied for the modeling of axial fans in the presence of inlet distortions. The numerical code was validated with the experimental data for the single passage clean inlet case. The same methodology was applied for the analysis of the boundary layer ingestion. The grid independence, boundary conditions, and numerical setup are also described. The methodology applied for the optimized rotor is also discussed in this chapter. The localized tip optimization is performed using a surrogate-based multi-objective genetic algorithm (MOGA). The Pareto front provided a set of non-dominated solutions from which the design point with the highest efficiency is selected for the optimized rotor.

References

[1] R. Wood, M. D. Hathaway, and K. L. Suder, "NASA Technical Paper 2879," 1989.

[2] B. L. Berrier, M. B. Carter, and B. G. Allan, "High Reynolds Number Investigation of a Flush-Mounted, S-Duct Inlet With Large Amounts of Boundary Layer Ingestion," 2005.

[3] A. Javed, R. Pecnik, and J. P. Van Buijtenen, "Optimization of a Centrifugal Compressor Impeller for Robustness to Manufacturing Uncertainties," J. Eng. Gas Turbines Power, vol. 138, no. 11, 2016, doi: 10.1115/1.4033185.

Chapter 5

Results and Discussion

5.1 Model validation

The model has been validated by generating the compressor map from choke to stall point at three rotational speeds of 100%, 90%, and 80% as shown in Fig. 12. CFD data shows good agreement with the experimental data. Since the blades of the rotor are not the replica of that used for experimentation, there is a slight reduction in the choke mass flow rate. At part speeds, the stall mass flow rate is lower, and the efficiency is higher for the experimental data than CFD. This is maybe due to the mismatch in the velocity triangles at the part speed which is also in common with some other published data. Figure 11 shows the total pressure ratio and total temperature ratio across the blade span. The total pressure

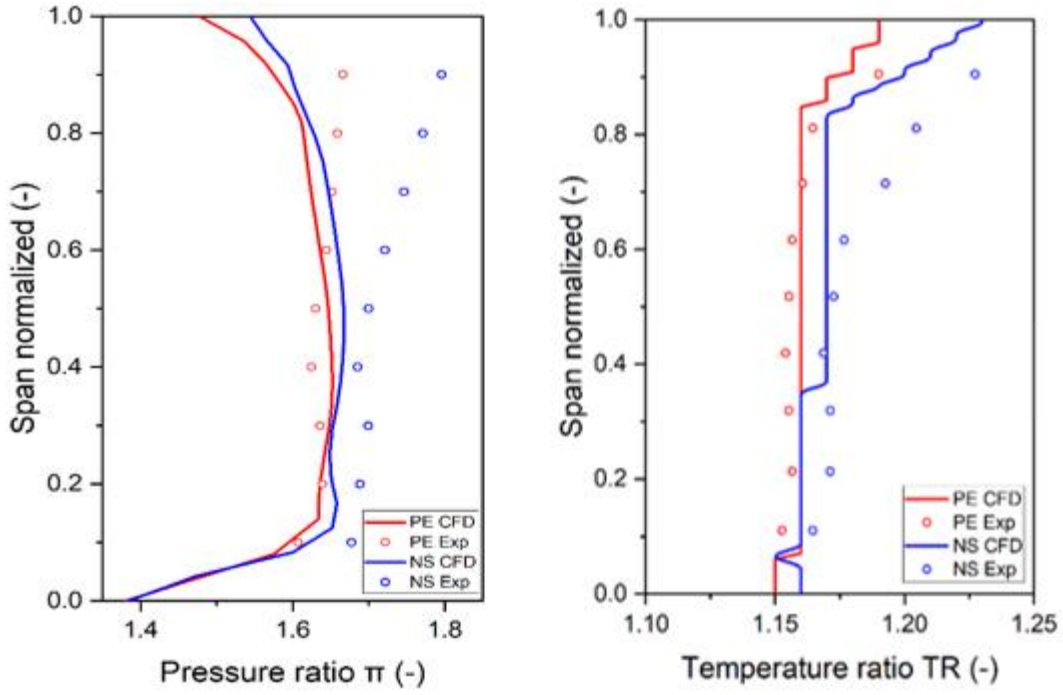

Figure 5.1: Radial total pressure and total temperature ratio for peak efficiency (PE) and near-stall (NS) point

and total temperature at the rotor outlet are normalized with the inlet total pressure and total temperature. The pressure and temperature ratio near peak efficiency (PE) show

good agreement across the blade span but shows some deviation near the stall point (NS) near the upper half of the blade. This is due to the complex nature of the flow near the stall point and the inability of the solver to accurately capture it.

5.2 Baseline case

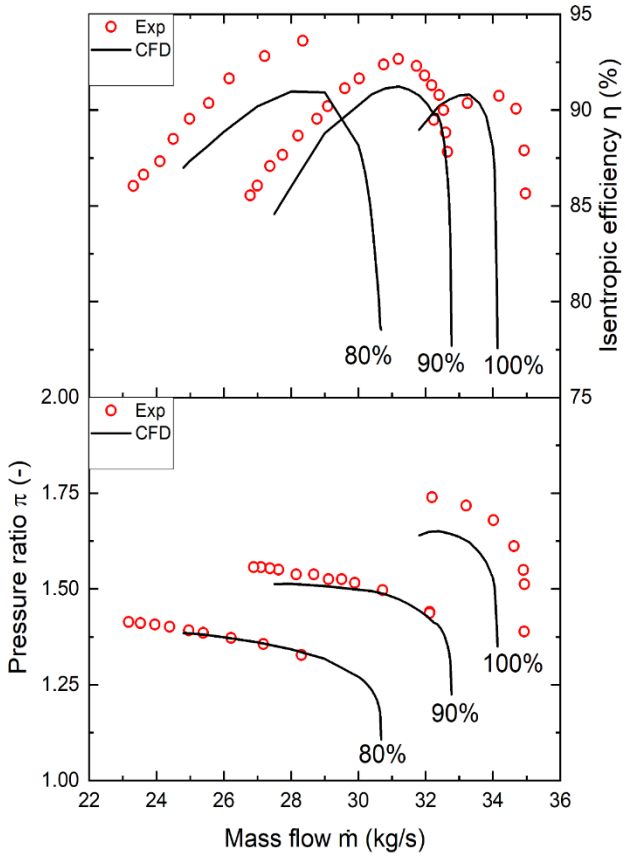

Figure 5.2: Rotor alone total pressure ratio and efficiency characteristics map for three different rotational speeds

5.2.1 Fan upstream flow field for inlet distortions

The flow reaching the fan face is no longer symmetric and has a circumferential distortion in total pressure, axial velocity, and swirl angle. The fan is no longer working at the design point. The fan is rotating at the design rpm but since the total pressure upstream of the fan is no longer uniform, there is a mass flow distortion as well. This means that each sector of the fan has a different mass flow passing through it. The rotor tends to attenuate this mass flow deficit. The regions of low mass flow rate tend to operate near stall thus giving slightly higher total pressure at the aft of the fan and as a result, static pressure upstream

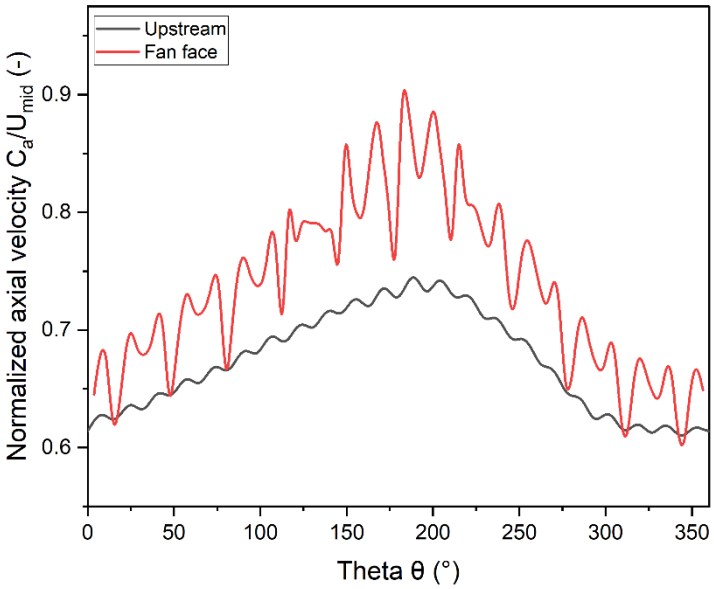

Figure 5.3: Circumferential distribution of axial velocity upstream of the fan and at fan face

of the fan is reduced. In other words, the fan sucks harder in the low total pressure region. This can be seen in Fig. 13. The velocity upstream of the fan is lower than that at the fan face. This clearly shows that the flow velocity increases in the vicinity of the fan. This increase in velocity results in decreasing the static pressure in the region. The difference between both the velocities is a maximum of around 180^{O}.

The nonuniform static pressure upstream of the fan causes a radial mass flow transport in which the flow goes from higher static pressure region to lower static pressure region This creates regions of co and counter swirling flow. Another factor inducing a radial flow is the interaction of the incoming flow and the spinner. In the absence of the incoming distortion, the stagnation point will be in the middle of the spinner. In the presence of distortion, as the flow gets slowed down while approaching the spinner, the distorted flow has a reduced static pressure than the clean flow, and the stagnation point is slightly shifted towards the clean sector. This imbalance causes the flow to migrate around the spinner. The spinner boundary layer also affects the flow before entering the fan. The velocity near the spinner wall is zero due to the no-slip condition and then increasing in the radial position. As the blade span increases, the intensity of the swirl decreases because of the reduced effect of the radial mass flow. The dark blue region in Fig. 14(d) shows high negative values of radial velocity indicating flow acceleration from tip to hub. As the fan

passes through regions of lower total pressure, local flow separation from the casing causes the formation of vortices.

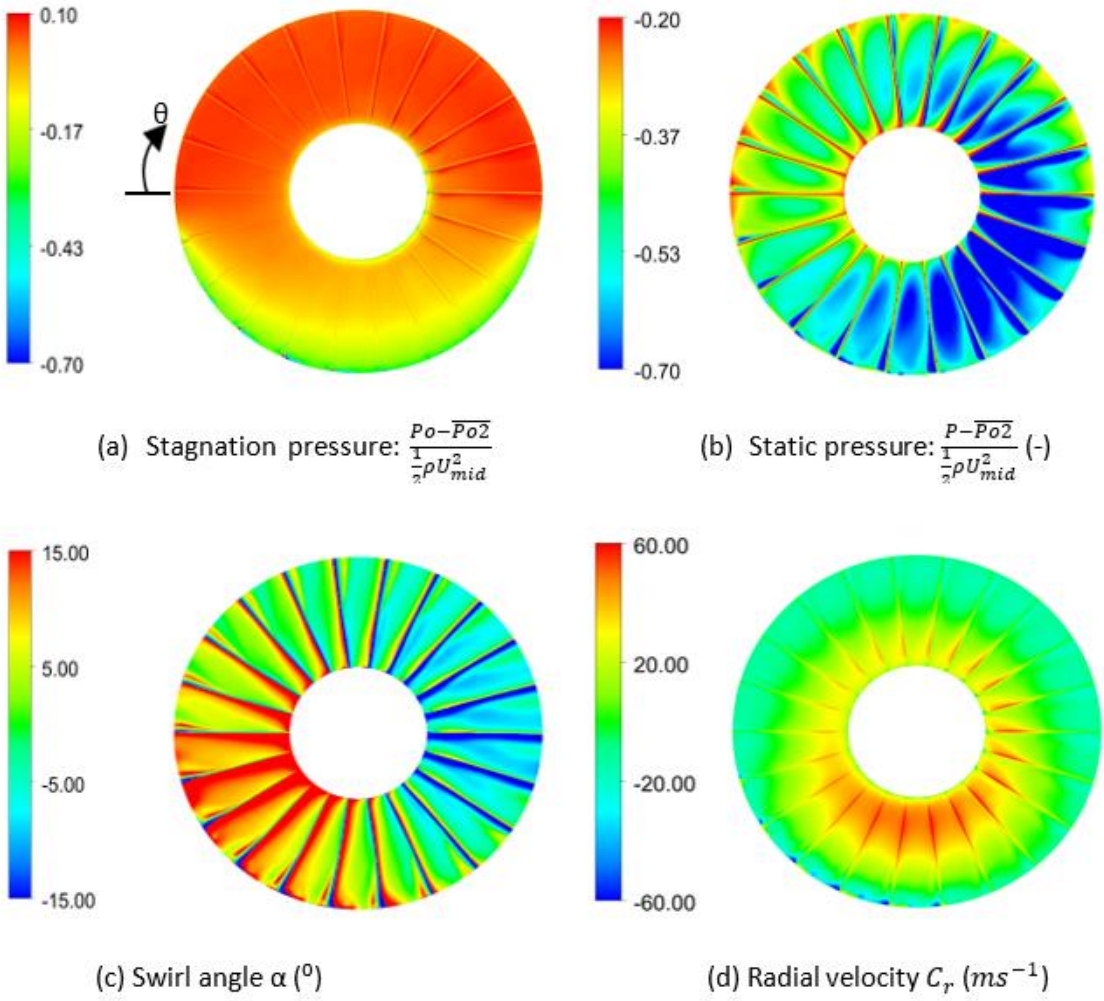

Figure 5.4: Flow properties at the fan face: (a) Stagnation pressure, (b) Static pressure, (c) Swirl angle and (d) Radial velocity

For the comparison of the BLI case and the clean inlet flow, the mass flow rate for the clean inlet has been normalized with the choke mass flow rate. The normalized mass flow rate of 0.992 is used for all the cases. The choke mass flow is calculated and then outlet static pressure is gradually increased until the desired normalized mass flow is achieved. The isentropic efficiency and pressure ratio reduce by 7.08% and 7.19% respectively.

5.2.2 Rotor flow distribution

Figure 16 shows the circumferential distribution of axial velocity at different spans. The circumferential distortion in axial velocity is greater near the hub as compared to other

radial positions. At the right side of the annulus, the axial velocity is higher near the hub. The flow redistribution continues within the rotor and the mass flow is fixed within each passage. At 70% and 90% span, the circumferential distortion is decreased within the rotor. But for a 30% span, the difference in the circumferential distortion is increased, this is due to radial mass transport near the hub. Due to flow distribution around the hub caused by static pressure difference, the radial velocity is highest around 270^{O}. The Figure shows that at the bottom half annulus, the radial velocity is high as compared to the upper half annulus. This radial velocity affects the fan performance and reduces the fan efficiency as explained in the later section.

The flow distribution across the whole annulus is to remove the mass flow deficit caused by the nonuniform total pressure profile upstream of the fan. This 3D flow distribution causes nonuniformities in axial velocity, swirl angle, and incidence angle. Figure 15 shows the circumferential distribution of swirl angle and incidence angle upstream of the fan. The region near the hub has high intensity of co and counter-swirling flow. The swirl is induced by the radial mass transport of flow around the spinner. The incidence angle depends on axial velocity and the swirl angle. Due to radial mass transport near the hub, the swirl angles are high. This combined with the high axial velocity causes the fan to continuously operate in negative incidence. From the hub to the casing, the axial velocity drops and so does the swirl angle due to the reduced effect of the radial mass transport. This results in reducing the negative incidence for 70% and 90% span but due to the presence of swirl the average incidence angle remains negative. But 90% span has a lower value of negative incidence than the 70% span due to the reason explained above.

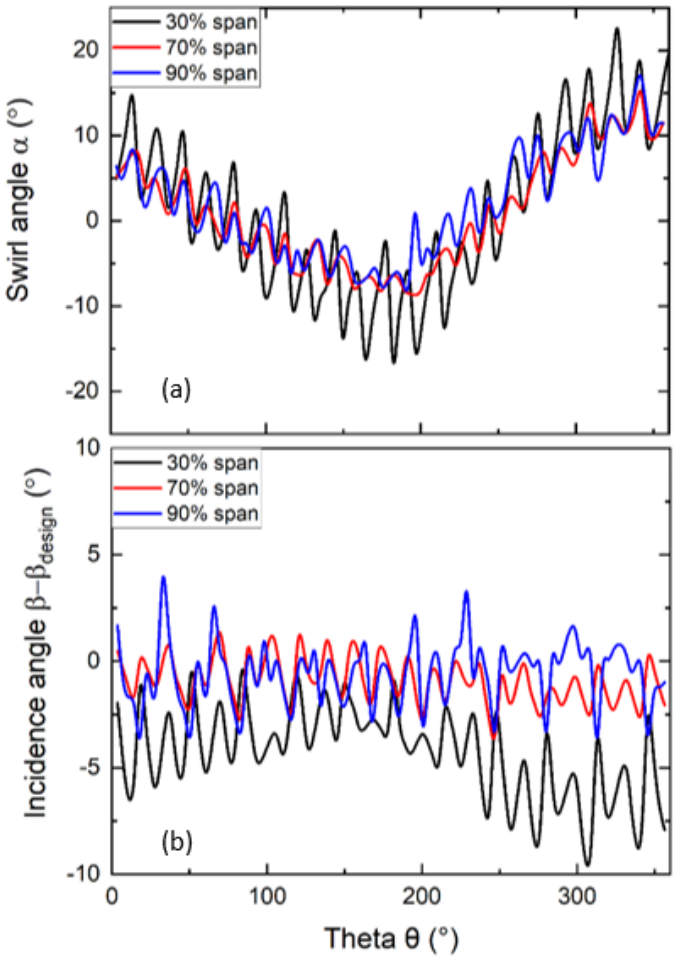

Figure 5.5: Circumferential distribution of: (a) swirl angle, and (b) incidence angle at fan face

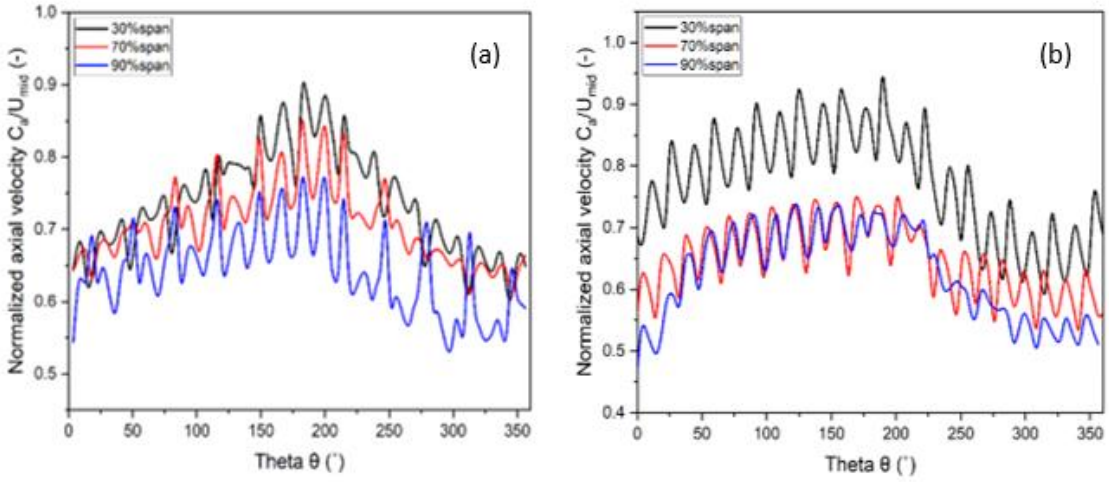

Figure 5.6: Circumferential distribution of axial velocity (a) upstream and (b) downstream of the fan

Figure 17(a) shows the temperature ratio (TR) of the fan which also gives an insight into the amount of work done by the fan. As the flow properties are not uniform across the fan face, the work distribution is also nonuniform. The work done primarily depends on axial velocity and incidence angle. As we move in the direction of increasing theta from 0^O the TR starts to increase to a maximum value and then starts decreasing. The region of highest TR lies in the region of high counter-swirling flow and low to medium velocity. As the rotor moves from the counter swirl region to the co-swirl, the negative incidence starts to increase again which starts reducing the work input. A similar pattern can be seen near the casing. In the lower annulus near the casing, there is a region of the highest TR. The fan is going from counter to co-swirl region which tends to reduce the angle of incidence, but axial velocity is low near the casing which reduces the negative incidence and thus increases the work done. The negative incidence angle starts increasing from 270^O to 360^O as the fan enters the region of co-swirl which reduces the work input. Near the casing around 0^O, the TR is the lowest. This region has the highest values of co-swirl flow which makes the incidence angle negative thus reducing the TR. As the rotor moves from co to counter swirl the negative incidence angle starts reducing and thus the TR starts to increase. A similar pattern can be seen with the total pressure ratio. The regions with high-temperature ratios also have high-pressure ratios and vice versa.

The entropy contours in Fig. 17(c) show that the entropy is the highest in the hub and the shroud region. These regions also have reduced efficiency and suffer the most. Near the casing, the downstream static pressure increases as the flow pass through a shock wave. The viscous layer attached to the casing has a lower momentum and the boundary layer gets thickened due to adverse pressure gradient. This boundary layer when detaches from the casing mixes with the mainstream flow causing increased losses, and thus the entropy increases. The entropy in the lower half annulus of the fan is higher as compared to the upper half annulus. As the flow moves along the curvature of the duct, the flow gets separated due to an adverse pressure gradient. This separation causes a region of low-velocity flow. As the flow approaches the fan face there is a formation of vortex in that region. This vortex combined with the tip leakage flow results in an increase in entropy.

The increased entropy near the hub is due to flow separation. The increased negative incidence reduces the flow turning thus causing the flow separation at the trailing edge.

Figure 17(d) shows the efficiency downstream of the rotor. The efficiency varies smoothly around the annulus up to around 80 % span. There is a region of reduced efficiency in the lower annulus of the fan near the hub. As shown in fig. 14(d), this region has high radial velocities which change the overall work distribution. The incidence angle is negative at a 30% span across the whole annulus. As the rotor enters the region of high radial velocity, the efficiency starts decreasing. The minimum efficiency is at 270^{O} where the radial velocity is maximum. The negative incidence angle increases from 180^{O} to 360^{O} due to the high co-swirl. Although the efficiency starts to improve as the rotor leaves the region of high radial velocity. This shows that incidence angle alone cannot give enough information about rotor efficiency. The band of low efficiency near the casing is caused due to flow separation. From 0^{O} to 180^{O} the thickness of this band nearly remains constant but starts to decrease as the negative incidence angle starts to reduce. This shows that the efficiency improves. But from 270^{O} to 360^{O} the thickness again starts to increase as the negative incidence starts increasing again.

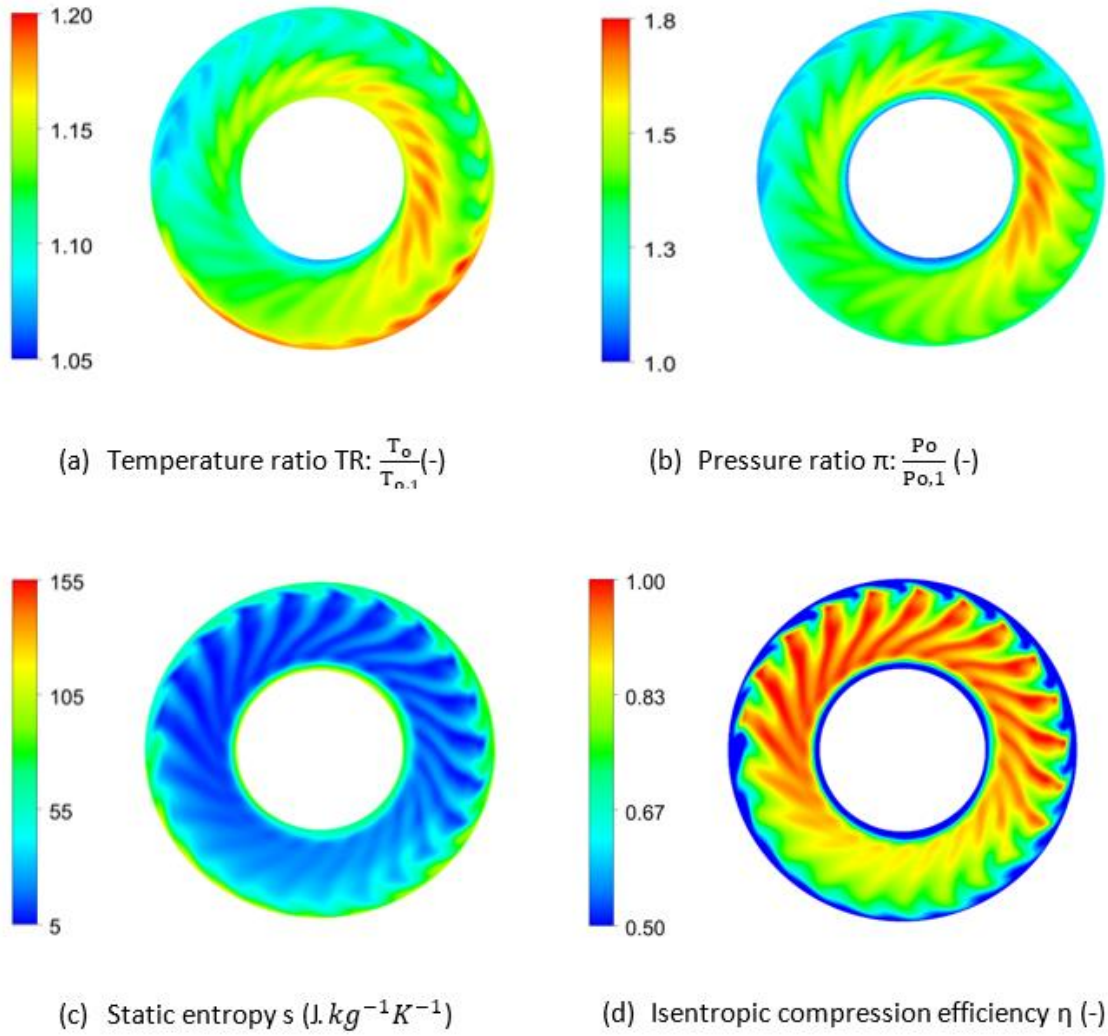

(a) Temperature ratio TR: $\frac{T_o}{T_{o,1}}$(-)

(b) Pressure ratio π: $\frac{Po}{Po,1}$ (-)

(c) Static entropy s ($J.kg^{-1}K^{-1}$)

(d) Isentropic compression efficiency η (-)

Figure 5.7: Temperature ratio, pressure ratio, static entropy, and isentropic compression efficiency downstream of the rotor

5.3 Optimized rotor

5.3.1 Comparison for Baseline and Optimized Case

The upstream flow field is dependent on the design of the fan blades. As the optimized fan is no longer the same as that of the baseline, this affects the upstream flow field. The upstream total pressure and static pressure for the optimized case are nearly the same as that for the baseline case. Figure 18 shows the circumferential distribution of incidence angle, normalized axial velocity, and swirl angle for optimized and baseline fan for 30%, 70%, and 90% span. The swirl distortion is produced by the mass transport from the high-pressure region to the low-pressure region. As the static pressure flow field is nearly the same as that for the baseline, the swirl angle is also the same for both cases. The incidence angle is a function of swirl angle and axial velocity. The swirl angle nearly remains the same around the annulus for both cases, but the axial velocity is different. The axial velocity for the optimized case is slightly less than the baseline in the upper annulus but as the blade enter the distorted sector there is a large velocity deficit going from 180^{O} to 270^{O} which gets maximum at around 270^{O} and then start reducing but overall, the velocity for the optimized case is lower than the baseline everywhere around the annulus. Since there is no significant change in the swirl angle, this reduced velocity increases the angle of incidence. For the baseline case the incidence angle varied but on average it was

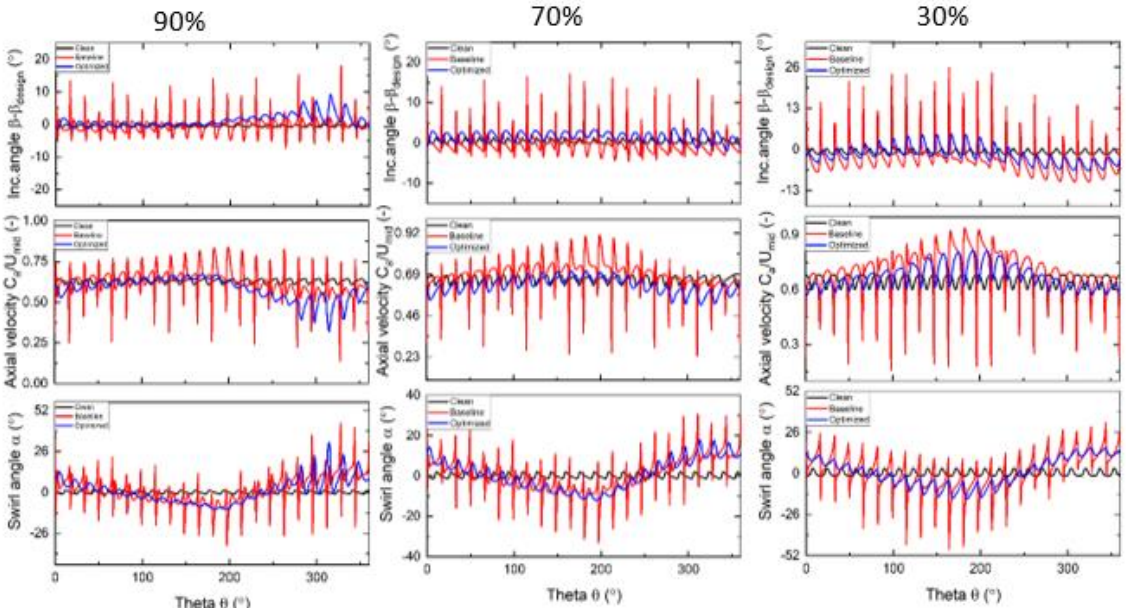

Figure 5.8: Comparison of rotor upstream flow field for clean, baseline, and optimized case at 90%, 70% and 30% span

negative. For the optimized case the incidence angle is positive on average. It can also be seen that the optimized fan has a more uniform upstream flow field than the baseline case with reduced fluctuations. This can be seen for all radial heights.

Figure 5.9(a) shows the temperature ratio (TR) downstream of the rotor for both the baseline and the optimized case. The work done by the fan is non-uniform around the annulus due to the swirl angle distortion. Near the casing, starting from 0^O the work done starts to increase as the fan moves from co-swirl to counter-swirl but then starts to decrease from 270^O as the fan enters in co-swirl again but since the velocity is low, the incidence angle is positive. The positive incidence flow gets higher work transfer as the flow accelerates more on the suction surface of the blade but for transonic compressors, such high positive incidence angles are detrimental and cause high shock losses and reduce work transfer.

Figure 19(b) shows the contours of the total pressure ratio. As compared to the baseline case, the pressure ratio for the optimized fan is 4.95% higher. This difference is due to the slight improvement in the blade leading edge angle which causes the incidence angle to become positive. The average incidence angle in the upper annulus of the fan is very close to zero in contrast to the baseline fan in which the incidence angle is negative on average. The work done and pressure ratio follows a similar trend. The pressure ratio is higher in the region in which the fan imparts more work to the incoming flow and as the work done starts to reduce due to the increasing incidence angle the pressure ratio starts to reduce.

Figure 19(c) shows static entropy downstream of the fan. The high entropy region near the hub is due to the shock-induced boundary layer separation. There is a high loss region near the tip around 180^O. This region has the highest axial velocity and the shock wave that is formed interacts with the blade boundary layer resulting in the formation of thicker wakes in that region. The casing boundary layer thickens while progressing through the rotor, but it doesn't separate as for the baseline case. The tip flow is sensitive to tip clearance. The tip clearance for the optimized fan is lower than the baseline case and an improved tip performance can be seen. The static entropy for the optimized fan is relatively lower than the baseline in the lower annulus of the fan.

Figure 19(d) shows the isentropic efficiency for the optimized fan. There is a region of low isentropic efficiency near the hub which is caused by shock-induced boundary layer separation. Near the casing, the thickness of the low isentropic efficiency band increases from 90^O to around 180^O. The shock wave formed due to the increasing velocity generates higher profile losses due to the boundary layer separation. It can also be seen that the static entropy is also the highest in that region. From 180^O to 270^O the width starts to reduce, showing an improvement in tip performance. The reduction in axial velocity causes the shock wave to move upstream. This significantly reduces profile losses due to boundary layer reattachment, reducing the wake. From 270^O to 360^O, the isentropic efficiency band nearly remains constant. There are a few lumps of low-efficiency regions where the incidence angle peaks cause high losses.

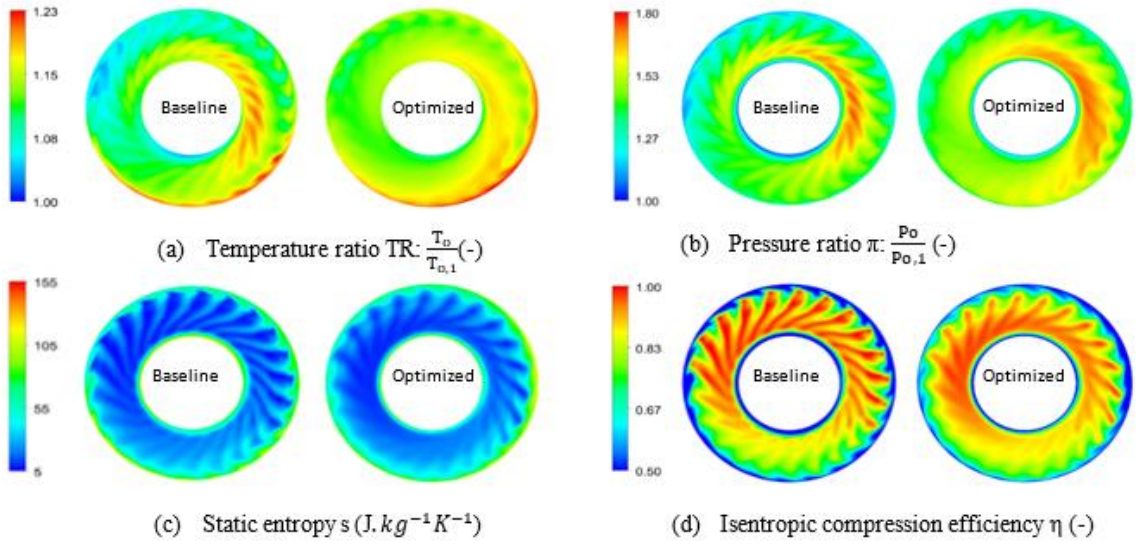

Figure 5.9: Comparison of temperature ratio, pressure ratio, static entropy, and isentropic compression efficiency between baseline and optimized fan downstream of the rotor

Figure 20 shows the comparison for swirl angle, normalized axial velocity, and total pressure ratio downstream of the fan at 30%, 70%, and 90% span for the optimized and the baseline case. The clean inlet case, in which there is no s-duct, is used as a reference to compare with the baseline and optimized case. The optimized fan has a more uniform downstream flow field at all radial heights. The downstream flow field for 90% span is more like that of a clean inlet case with relatively small distortion and reduced fluctuations. From the shroud to the hub the downstream circumferential distortion

increases but is in close vicinity to the clean inlet case and but has an improved performance than the baseline case. The optimized rotor with an improved tip performance affects the whole flow field across the blade span indicating the flow redistribution for an overall improved performance

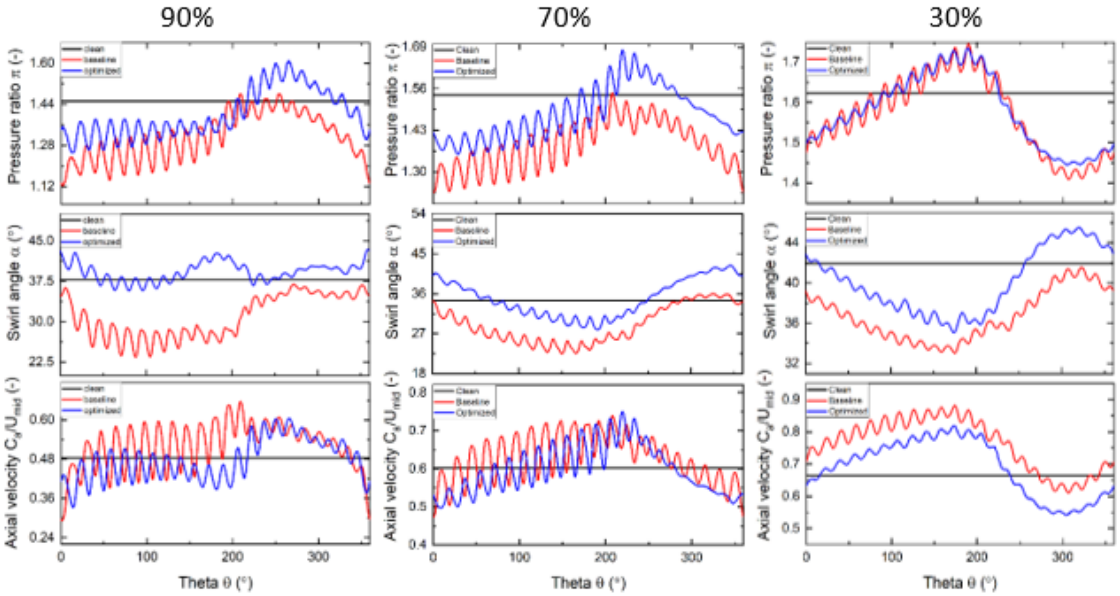

Figure 5.10: Comparison of rotor downstream flow field for clean, baseline and, optimized case for 90%, 70% and 30% span

5.3.2 Blade to Blade Distortion Transfer

Figure 21 shows blade to blade contours of temperature ratio and Mach numbers at 90% span. The distortion region is shown within the dotted lines. The position of the shock wave is highly dependent on the inlet mass flow passing through each blade passage. The undistorted region has high mass flow than the distorted region. The shock wave is well swallowed within the passage which can only be seen in fans operating in clean flow conditions near choke. The inlet relative Mach number in the distorted flow is lower and the shock wave moves upstream near the leading edge of the blade combining with the bow shock at the leading edge and forming a stronger shock wave. These types of shock waves can be seen in fans operating in near-stall conditions. The shock waves interact with the blade boundary layer thus causing separation and increasing losses. For the undistorted region, the shock waves are formed near the trailing edge of the blade and interact with the pressure surface boundary layer of the adjacent blade causing it to separate. The flow does not completely reattach with the blade profile and a thick wake

can be seen downstream of the fan. As the blade passes through the distorted sector the shock moves upstream causing flow separation on the blade suction surface. The flow reattachment can be seen which reduces the overall wake losses. The overall losses near the casing are caused by the interaction of the shock waves with the blade boundary layer and casing boundary layer. There also exists the Mach number distortion downstream of the rotor. The clean region with high total pressure has a high axial velocity as compared to the distorted sector. The flow in the distorted sector receives higher work input which means that higher flow turning. In transonic compressors, near the tips of the blades, the diffusion is caused by the help of shock waves rather than using flow turning in subsonic compressors. As described above that in the distorted sector the shock gets stronger and moves upstream. As the flow passes through the shock the whirl velocity is lower which is necessary to achieve higher diffusion. This reduced velocity results in higher absolute whirl velocity. It can be seen in Fig. 21(a) that the high Mach numbers correspond to the distorted sector. The opposite can be said for the clean sector in which the absolute whirl velocity is lower. This non-uniform velocity distribution can create higher losses in the stator.

TR contours show that the highest work done by the fan is in the distorted sector due to reduced mass flow. As the fan enters the distorted sector, the counter swirl starts to increase which improves the incidence angle thus improving the work done. As the fan enters the clean sector the TR is lower. This is due to high values of co-swirl which reduces the overall work transfer.

The shock wave structure for the optimized case is slightly different than the baseline case due to the difference in axial velocity and incidence angle. The axial velocity for the optimized case is slightly less than the baseline across the annulus which causes the shock waves to move upstream. At around 180^{O}, the optimized case has a thicker wake due to the shock wave boundary layer interaction. The boundary layer separates from the suction surface and generates thicker wakes but the overall work transfer is higher than the baseline case due to the improved incidence angle. In the distorted sector for optimized case, a high Mach number can be seen before the shock wave as compared to the baseline. This is due to the flow acceleration on the suction surface of the blade due to positive

incidence. This also results in a high value for temperature ratio indicating more work done by the rotor.

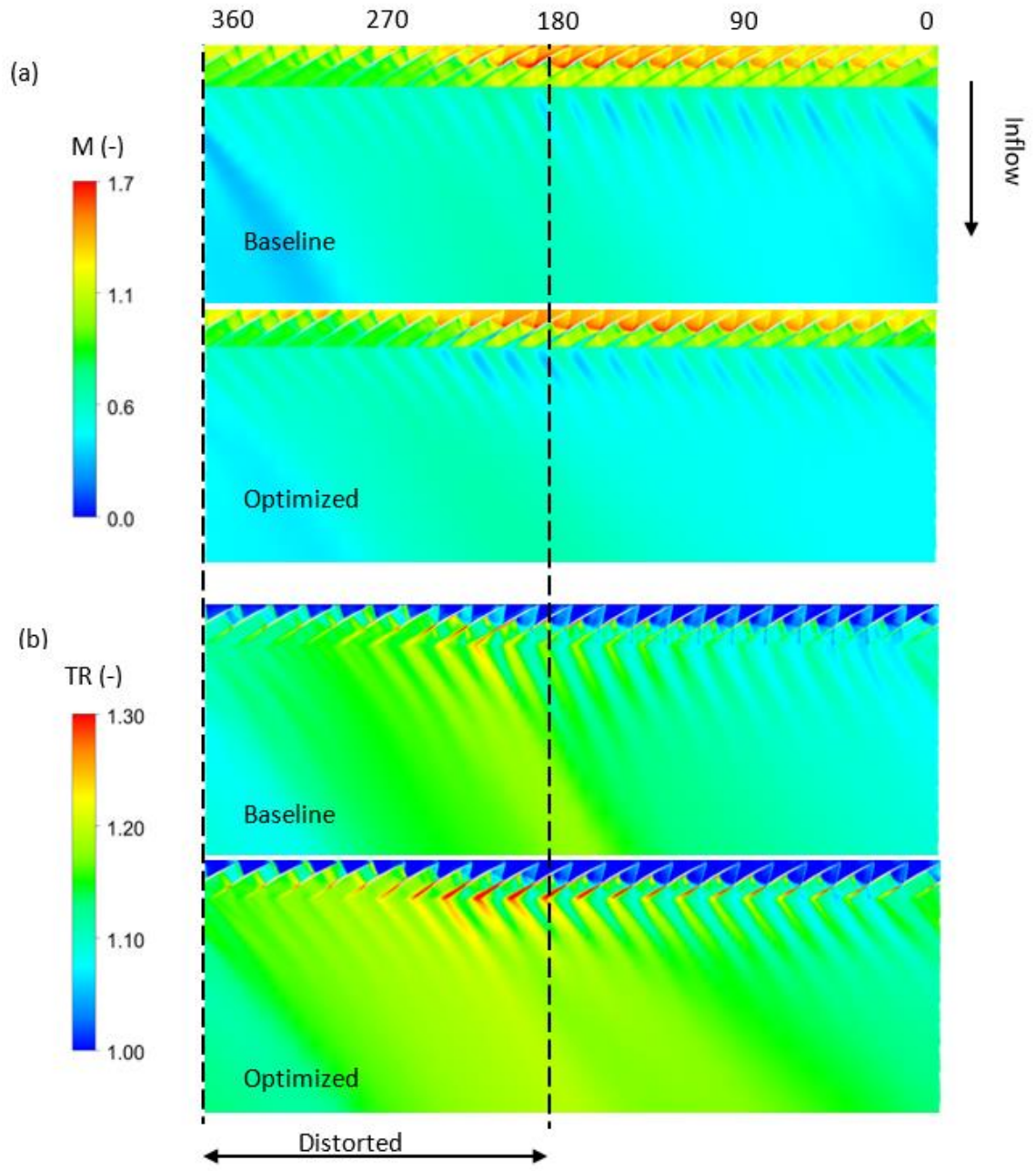

Figure 5.11: Unwrapped blade to blade snapshots for (a) Mach number and (b) temperature ratio for baseline and optimized case at 90% span

Summary

This chapter presents the detailed analysis and comparison of the rotor upstream and downstream flow fields for the baseline and optimized case. The upstream distortions significantly change the upstream flow field variables. The work input of the rotor is highly dependent on the swirl angle and the axial velocity. The circumferential distortion in both these variables causes the rotor to produce non-uniform work distribution across the whole annulus. The rotor is no longer working in its design condition. The tip of the rotor has higher losses due to the shock wave boundary layer interaction which can be seen to be significantly reduced for the optimized rotor due to the reduced tup clearance. The improved leading-edge angle also causes the rotor to show a better incidence angle profile for the optimized rotor which improves the work done by the rotor hence the optimized rotor has a pressure ratio than the baseline fan. Moreover, it was also found out that altering the tip profile also has an effect on the flow field across the whole span and the optimized rotor has an improved downstream flow field than the baseline case.

Chapter 6

Conclusions and Recommendations

6.1 Conclusions

The aerodynamics of NASA Rotor 67 attached with an s-duct featuring inlet distortion is studied using full annulus, steady-state CFD simulations. The numerical CFD code is validated with the experimental data available in the open literature.

The flow field is no longer axisymmetric and severe swirl angle and axial velocity distortion exist upstream of the rotor. The intensity of swirl distortion decreases moving from hub to shroud. The swirl distortion affects the overall work distribution and the local operating point of each blade passage across the complete fan face. This leads to a non-uniform flow field downstream of the rotor. This also affects the overall shock wave structure in the rotor.

The localized tip optimization is performed to redesign the rotor that has a more uniform downstream flow field and an improved tip performance as compared to the baseline case. Leading-edge angle, trailing edge angle and tip clearance is used to parametrize the rotor tip for optimization.

The surrogate model-based multi-objective genetic algorithm is employed to obtain the Pareto front of non-dominated solutions with improved output response variables as compared to the baseline case. The suitability of the surrogate is validated by comparing the CFD solution with the surrogate solution. The optimized fan corresponds to the rotor with a reduced tip clearance as compared to the baseline case. A sensitivity analysis performed showed that the isentropic efficiency is sensitive to tip clearance while the pressure ratio is sensitive towards the leading-edge angle and tip clearance.

The optimized rotor has an improved pressure ratio and isentropic efficiency with an improved downstream flow field indicating the optimized rotor is more distortion tolerant. The localized tip optimization also affects the flow field across the whole blade span and an improved flow field is observed at all radial heights as compared to the baseline case.

This paper serves as a baseline for future studies of boundary layer ingesting propulsion systems. Full annulus, unsteady CFD simulations can help in better understanding the flow physics inside the blade channels and account for the loss sources. This paper presents localized tip optimization of NASA rotor 67 which can be extended in the future featuring the full 3D design modification of the whole blade designing a more distortion tolerant fan that can work efficiently in the presence of inlet distortions without any loss in thrust, efficiency, and stability of the fan.

6.2 Future prospects

This study presents the effect of the boundary layer ingestion on the fan performance and the rotor flow field. The efficiency of the fan suffered the most. This study although presented that redesigning the rotor will help improve the rotor flow field and efficiency but this study was only limited to the localized tip optimization. The prospect includes localized optimization for some other span location or can also redesign the whole blade from hub to tip.

There is very little amount of research done on redesigning the duct to reduce the flow separation from the duct curvature and reduce the secondary flows to reduce the distorted sector upstream of the rotor. This can also be done by introducing the doorways around the periphery of the duct from which the low-velocity flow can be sucked out to reduce the low-pressure region caused by this flow or high-velocity flow can be introduced through these gateways to energize the low momentum flow and reduce the distorted region upstream of the fan.

Acknowledgment

Firstly, I would like to thank Allah Almighty for providing me knowledge, determination, opportunity, and strength to complete this venture. Without His blessings, all of it would not have been possible.

I would like to express my gratitude to my supervisor Dr. Adeel Javed for allowing me to conduct my thesis under his supervision.

I also want to thank my GEC committee members Dr. Majid Ali, Dr. Adnan Maqsood, and Dr. Adeel Waqas. I feel proud and honored that you have accepted to be on my committee.

Finally, and most importantly, I express my profound gratitude to my parents for providing me with unfailing support and continuous encouragement throughout my years of study and through the process of researching and writing this thesis.

Appendix

A.1 Publication 1

Parametric Optimization of NASA Rotor 67 Transonic Tips for Improved Localized Distortion Tolerance against Boundary Layer Ingesting Flows

Talha Bin Tahir[a], Adeel Javed[a,1], Adnan Maqsood[b]

[a] Thermal Energy Engineering Department, U.S.-Pakistan Center for Advanced Studies in Energy, National University of Sciences & Technology, H-12 Islamabad

[b] Research Center for Modelling and Simulation, National University of Sciences & Technology, H-12 Islamabad

Abstract

The robust performance of transonic fans in the presence of inlet distortions for boundary layer ingesting aircraft poses significant design challenges. This paper presents a numerical optimization strategy for distortion tolerant transonic fan design featuring an improved interaction between the transonic fan tips and the upstream flow distortions. The NASA Rotor 67 has been used as a baseline case in this study, while the boundary layer ingestion has been numerically simulated using an s-duct inlet. As a result, the combined modeling of the NASA Rotor 67 and the s-duct are capturing the flow fields typically experienced by the propulsion systems of future blended wing body aircraft concepts. Full annulus, steady-state, three-dimensional modeling has been used for the combined analysis of the rotor and s-duct. The NASA Rotor 67 computational fluid dynamics model is validated by the experimental data available in the open literature. Results indicated that the isentropic efficiency and pressure ratio have reduced by 7.08% and 7.19%, respectively due to the inlet distortions. The flow redistribution upstream of the fan causes a non-uniform work distribution across the complete fan face. A localized multi-objective design optimization featuring a surrogate model-based genetic algorithm setup was then applied to the transonic rotor tips. The optimized rotor design resulted in improved overall performance and relatively stable operation under the influence of inlet distortions compared to the baseline. The findings indicate an overall stable operation under the influence of the upstream distortions across the blade span rather than just an improved tip performance.

Keywords: NASA Rotor 67, s-duct, inlet distortions, numerical analysis, multi-objective genetic algorithm (MOGA), localized transonic tip optimization

[1] Corresponding author: Dr. Adeel Javed, Associate Professor. Email: adeeljaved@uspcase.nust.edu.pk